# FAT QUASARS IN BOSS: A SAMPLE OF 220 QUASARS WITH BROAD EMISSION LINES AND OBSCURED CONTINUA IN THE SLOAN DIGITAL SKY SURVEY

Benjamin A. Cook

A JUNIOR PAPER
PRESENTED TO THE FACULTY
OF PRINCETON UNIVERSITY
IN CANDIDACY FOR THE DEGREE
OF BACHELOR OF THE ARTS

RECOMMENDED FOR ACCEPTANCE
BY THE DEPARTMENT OF
ASTROPHYSICAL SCIENCES

Adviser: Prof. Michael Strauss

May 3, 2013

## ABSTRACT

Quasars are the extremely luminous cores of galaxies, whose central super-massive black holes are rapidly accreting mass. Non-uniform dust obscuration is thought to lead some quasars to appear obscured or unobscured depending on our line of sight. In this work, we describe the development and analysis of a sample of 220 high redshift quasars ($z \gtrsim 2.0$) in the SDSS Baryon Oscillation Spectroscopic Survey database which do not fit cleanly into this obscured/unobscured framework. The CIV emission lines of these *fat quasars* are broad (FWHM $\geq 2000$ km s$^{-1}$), yet also have high rest-frame equivalent widths ($\geq 100$ Å) suggesting faint rest-frame UV continua. We visually inspected the spectra of all quasars in the sample, characterizing them according to observable spectral properties and confirming that these objects possess both obscured and unobscured characteristics. With data from the Wide-Field Infrared Survey Explorer on many of the objects in this sample, we additionally find that they radiate strongly in the infrared, compared to similar objects in the BOSS database. We believe these fat quasars may yield useful information about the "unification model" of quasar properties, as we search for a description of the physical phenomena which could explain these interesting objects.


## 1. Introduction

### 1.1. History and Basic Characteristics of Quasars

In 1963, an astronomical radio source was found by Dr. Maarten Schmidt to coincide with a faint optical point-source. The unresolved object, despite being far too small in angular extent to represent an entire galaxy, was consistent with a redshift of 0.158, suggesting that it was not a star as it appeared (Schmidt 1963). Objects similar to this "quasi-stellar radio source" became known simply as *quasars* and, as of today, they have been identified by the hundreds-of-thousands and have become inarguably one of the most useful classes of objects to the astronomer wishing to study the high-redshift universe.

Quasars are one class of Active Galactic Nuclei (AGN), which are the extremely luminous centers of particular galaxies. Emitting at nearly all wavelength ranges of the electromagnetic spectrum, from radio to optical to UV and X-Ray, AGN cannot be explained simply by blackbody or stellar processes. Instead, AGN are believed to be the result of rapid accretion of gas onto the super-massive black hole (SMBH) of a large galaxy. Because the in-falling matter would initially come in with high angular momentum, it would likely escape the potential of the SMBH without coming close enough to be captured by the event horizon. Through interactions with other matter in the accretion disk around the black hole, angular momentum is removed from the accreting material, allowing it to spiral into the event horizon. Due to the viscous forces which contribute to

this angular momentum stripping, the kinetic energy which was lost by the accreting gas is converted into heat and extreme amounts of radiation, and it is this accretion disk which is believed to be responsible for the extreme luminosity ($> 10^{48}$ erg s$^{-1}$ in some cases) of these AGN.

AGN are classified into two broad categories: quasars (higher luminosity in all wavelength ranges) and Seyfert galaxies (lower luminosities), named after Carl Seyfert who first identified them in 1943. Quasars typically are those AGN with luminosity (in various bands) above $\sim 10^{44}$ erg s$^{-1}$ and in most cases easily outshine their entire host galaxies by orders of magnitude.

### 1.2. AGN Spectra

AGN (and hence quasar) spectra also often contain strong emission and absorption features, which are due to the intense energy of the AGN exciting nearby gas. This gas will re-radiate the absorbed photons at only specific wavelengths determined by the quantum structure of the elements which make up the gas: these features are called *spectral lines* and are unique to specific elements and ions. Depending on the conditions of the gas around the AGN, different spectral lines may appear prominently in the observed spectrum of an AGN. Two important spectral lines which will be used in this work are the Lyman Alpha line (Ly$\alpha$, the 2→1 electronic transition of neutral hydrogen) at 1216 Å, and the Carbon IV line (CIV, an electronic transition in triply-ionized carbon) at 1549 Å. The apparent width of the feature (usually modeled with a Gaussian distribution) comes from Doppler broadening, which is due to the internal random motions of the gas. The velocity dispersion ($\sigma_v$) of the gas is related to the Gaussian width (measured in the rest frame) of the line ($\sigma_\lambda$) via the Doppler Equation:

$$\frac{\sigma_v}{c} = \frac{\sigma_\lambda}{\lambda_0} \tag{1}$$

where c is the speed of light (3.0x10$^5$ km s$^{-1}$) and $\lambda_0$ is the rest wavelength of the line. The velocity dispersion is also commonly given in terms of the full-width at half-maximum (FWHM), which for a Gaussian distribution is simply

$$\mathrm{FWHM} = 2\sqrt{2\ln 2}\,\sigma_v\,. \tag{2}$$

Gas which is deeper in the potential well of the SMBH must have higher velocities in order to stabilize (from the Virial Theorem), so the velocity dispersion of lines can often be taken as a rough proxy for the proximity of the emitting gas to the central engine of the AGN. An additional parameter which can characterize a spectral feature is its *equivalent width* (EW), measured in Å. The equivalent width is given by:

$$\mathrm{EW} = \left| \int \left(1 - \frac{F_\lambda}{F_0}\right) d\lambda \right| \tag{3}$$

where $F_\lambda$ is the measured flux over the region of interest and $F_0$ is the continuum flux level in that region. For emission, the EW is connected to the total line flux relative to the continuum.

The overall radial velocity of the galaxy which houses the quasar introduces a systematic redshift to the entire spectrum, as a result of the expansion of the universe. Thus, AGN at large distances from the Milky Way will have large redshift values (z), and all spectral lines will be Doppler shifted from their rest positions by

$$\lambda_{observed} = \lambda_0 \, (1 + z) \tag{4}$$

often bringing short-wavelength lines into the optical regime when observing from Earth. The Lyman Alpha line, for instance, is in the UV at rest, but is shifted into optical wavelengths above redshift z = 2.0.

### 1.3. Obscured Quasars and the Unification Model

AGN of the two classes (quasars and Seyferts) are also found to be classifiable into further subclasses: Type I and Type II. Type I AGN exhibit broad spectral features (FWHM up to $10^4$ $\mathrm{km\,s^{-1}}$) and strong, blue continua in the optical and UV. In contrast, Type IIs are characterized by narrow lines (FWHM $\lesssim$ 1500 $\mathrm{km\,s^{-1}}$) and weak, flat continua in the ultraviolet and optical. See Fig. 1 for a side-by-side comparison of the spectra of a Type I and a Type II quasar.

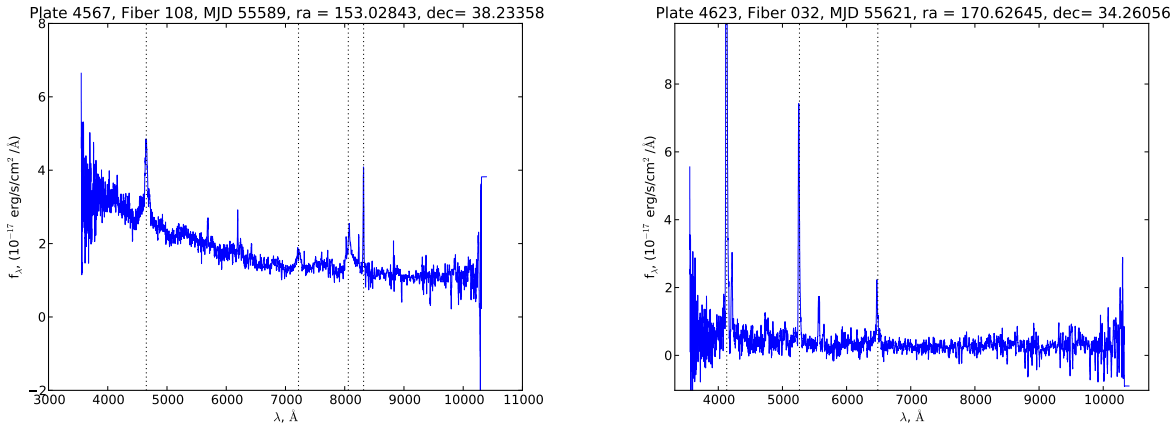


Fig. 1.— *Left*: The BOSS spectrum of a quasar, identified by Bolton et al. (2012) to have a redshift z = 0.661. Note the characteristic blue slope of the continuum and the broad emission lines. These properties clearly identify the quasar as Type I. The spectral lines identified are, from left to right: MgII, H$\gamma$, H$\beta$, and [OIII]. *Right*: Another quasar, redshift z = 2.393. Compare its flat, faint continuum and narrow spectral features to the Type I to the left. This object has been classified by Alexandroff (2012) as an example of a high-z Type II quasar. The spectral lines identified are, from left to right: Ly$\alpha$, CIV, and CIII]. Lines identified through consultation of Vanden Berk et al. 2001.

These observed properties of AGN have led to the development of a *unification model* to

explain the dichotomy between Type I and Type II. It is theorized that AGN may be surrounded at moderate distance by a non-uniform cloud of thick dust, often envisaged as a torus. If our line-of-sight to the AGN did not intersect the dust, then we would be likely to observe the bright blue continuum and strong, broad spectral features as outlined in the general picture of AGN above. If, however, the dust obscured the quasar from our direct sight, then much of the ultra-violet and optical continuum may be absorbed away and re-radiated in the infrared.[1] This picture of AGN obscuration leads to a physical explanation for the differences between unobscured (Type I) and obscured (Type II) AGN (Zakamska et al. 2003). Furthermore, if the high-velocity gas emissions were also obscured from sight, then observed emission lines could be narrower, coming from slower-moving gas clouds in the regions of shallower potential. The so-called broad-line region (BLR) is predicted to be on smaller scales than the size of the dust-torus, while the narrow-line region (NLR) is found on larger scales visible despite the obscuring dust. Light from the central engine could excite gas in the NLR and narrow-line emission could be scattered back into our line of sight.

Thus, the unification model suggests that the observed properties of an AGN may be determined in large part by the obscuration of the central engine and our viewing angle. If our viewing angle lies near the plane of the dusty torus, the AGN will be heavily obscured, and we would classify the object as a Type II, while an angle perpendicular to the plane of the torus would leave the AGN unobscured (Type I). Recent works have claimed that AGN may instead go through an initial obscured phase, until the dusty layer is blown away by the central engine, and the AGN is left unobscured (Hopkins et al. 2006).

For her senior thesis project, Princeton undergraduate Rachael Alexandroff discovered and characterized a sample of high-redshift Type II quasars in the Sloan Digital Sky Survey (SDSS) Baryon Oscillation Spectroscopic Survey (BOSS). As part of this work and subsequent analysis, Alexandroff identified four objects with interesting properties, which did not fit precisely into either category Type I or Type II. These objects were noted for their faint continua in the rest UV, and were found by the Wide-Field Infrared Survey Explorer (WISE) to emit strongly in the IR, indicating they were likely obscured. Yet these objects also had broad emission lines (FWHM $>$ 3000 $\mathrm{km\,s^{-1}}$), characteristic of unobscured Type I quasars (Alexandroff et al. In Preparation).

Throughout this work, we will describe a project which was undertaken during the spring of 2013 to learn more about these broad-emission-line, faint-continuum quasars, which we will refer to often as "fat quasars." In particular, the focus was on identifying other quasars in BOSS with similar properties, and attempting to characterize them as a population. In §2 of this paper, we outline SDSS and the BOSS survey. In §3, we analyze two different sources of data relevant to quasars and compare their utility. §4.1 describes the process of selecting a sample of quasars to match the fat quasars found by Alexandroff, and in §4.2 we inspect the spectra of the objects in

[1]Large molecules which form in dust clouds have more complicated vibrational and rotational energy transitions available at low energies. For this reason, a dust grain may absorb an energetic UV or optical photon, and re-radiate the energy in the IR through several available low-energy modes.

this sample, eventually reaching a final count of 220 objects which match the description of faint continuum and broad emission lines. §5 further characterizes the optical and IR properties of the finalized sample, in comparison to BOSS quasars on the whole. Additional details on our sample are provided in Appendix A

All computation was performed in Python, using Numpy, Scipy, and PyFITS packages. Images were created using the Python package matplotlib (Hunter 2007).

All spectra shown in this work are smoothed using a five-pixel boxcar method. Because spectral features narrower than two pixels across will be unresolved, this smoothing allowed improved visual analysis of the wider features without any loss of information.

## 2. Data Acquisition

### 2.1. The Sloan Digital Sky Survey Baryon Oscillation Spectroscopic Survey

Begun in 2000, SDSS (Gunn et al. 1998; York et al. 2000; Gunn et al. 2006; Ahn et al. 2012) is an ongoing astronomical survey, which has become one of the largest and most productive projects in the history of astronomy. Centered at the Apache Point Observatory in New Mexico, the main instrument used in the survey is a 2.5 meter reflecting telescope, which is equipped for both wide-field imaging and spectroscopic analysis of individual objects. The first two phases (SDSS-I 2000-2005 and SDSS-II 2005-2008) imaged over 12,000 square degrees of sky, obtaining spectra for over a million galaxies and quasars and almost half a million stars.[2] All scientific data from SDSS-I/II was released both to the scientific community and the public in annual Data Releases, culminating with Data Release 7 upon the completion of SDSS-II.

The latest iteration of the Sloan Survey is SDSS-III, a six-year program which began in 2008 and is scheduled to continue through 2014 (Ross et al. 2012). SDSS-III also uses the Sloan Foundation 2.5 meter telescope to carry out four surveys on three main themes: the study of dark energy and cosmological parameters of the universe, the makeup and evolution of the Milky Way, and the architecture of planetary systems. Continuing the open tradition of SDSS, data produced from SDSS-III is released to the public regularly, including Data Release 8 in January 2011 and Data Release 9 in August 2012 (Ahn et al. 2012).

Comprising two of the four major SDSS-III surveys (and the project to which the most dark nights are dedicated), BOSS is a five-year program designed to measure the cosmic distance scale with exquisite precision and analyze the effects of dark energy. BOSS performs high-resolution spectroscopy (median $R = \lambda/\Delta\lambda \sim 2000$) on 1000 objects at a given time (Ahn et al. 2012). Large spectroscopic plates, on which holes are precisely drilled, hold the 1000 optical fibers for each object

[2]For more information on the incredible legacy of the first stages of SDSS, the author highly encourages readers to visit `http://www.sdss.org/signature.html`.

analyzed. The total wavelength coverage is from 3600 Å to 10400 Å, significantly widened from SDSS-I/II (Ahn et al. 2012). Throughout the project, BOSS will obtain spectra of over 1.5 million red galaxies in the redshift range $0.15 \lesssim z \lesssim 0.8$, and 150,000 quasars in the range $2.2 \lesssim z \lesssim 4.0$ (Eisenstein et al. 2011; Ross et al. 2012; Ahn et al. 2012). SDSS Data Release 9 (DR9) distributed to the public the first set of data collected by BOSS.

### 2.2. BOSS Pipeline Data Model

For this work, we relied upon data gathered by BOSS which is available in DR9. While data obtained after the release of DR9 in August 2012 is available to researchers associated with SDSS, such as this project's adviser Prof. Michael Strauss, our analysis relied significantly on the Data Release 9 Quasar catalog (see §3.1), which contains only data available as of the release of DR9. The newest data will be made publicly accessible with the distribution of Data Release 10, expected in July 2013 (Strauss, Michael; personal correspondence) and a continuation of this work with the data available from DR10 will hopefully improve the results gathered here.

Because the spectroscopy of BOSS is organized into plates (where one plate is drilled with 1000 holes for optical fibers), the data files are cataloged by plate number (a 4-digit integer), as well as Modified Julian Date (MJD), a five-digit integer specifying the date of observation. Individual objects observed on a particular plate are given an integer fiber number between 1 and 1000 to match which optical fiber was used to gather the spectrum of the object. Thus, data relating to a given object can be located given three pieces of information: the plate number on which the object was observed, the fiber number corresponding to the object itself, and the MJD when the data was taken. Additionally, different types of data (such as raw spectral data or processed fits to the data) are kept in different types of files. The collection of these data files will be referred to as the *BOSS pipeline*, to distinguish the original data analysis from later compilations (see §3.1). This work relied primarily upon a few specific types of pipeline data files, which are described in Appendix B.[3]

### 2.3. Flexible Image Transport System

All SDSS-III data files are kept in Flexible Image Transport System (FITS) form. FITS is the primary standard by which astronomers catalog and share data across any type of platform or software usage. The basic unit of a FITS file is a Header-Data-Unit (HDU), which is comprised of a user-readable ASCII header (which outlines the data held in the HDU in terms of header keywords) followed immediately by the binary data.

[3]For a complete list of the SDSS-III file structure, see `http://data.sdss3.org/datamodel/index-files.html`.

An individual FITS file may contain any number of HDUs, although the first in the file is known as the primary HDU, and any HDUs which follow are labeled extension HDUs. The data stored in the HDU can represent many types of information, such as digital images, binary tables, or ASCII text tables. This allows for incredible variety, as one FITS file could, for example, store a digital image of a field in its primary HDU, the spectra of selected objects in that field in the first extension, and spectroscopic parameters fit to those objects in the second extension. There are numerous ways to access the data contained in FITS files, and we relied upon PyFITS - a package for Python designed for easy manipulation of FITS files - throughout this work.[4]

## 3. Quasar Data Sources

### 3.1. Data Release 9 Quasar Catalog

In addition to the BOSS data files described in §2 and Appendix B which contain data on all objects observed by BOSS, a major source of data upon which we relied throughout our analysis was the Data Release 9 Quasar catalog (DR9Q) published by Pâris et al. (2012). This catalog is a single FITS file which contains data on almost every BOSS object which has been spectroscopically confirmed to be a quasar. The catalog contains data on 87,822 quasars collected over 3275 square degrees of the sky and served, among other uses, as our list of the population of all quasars observed in BOSS.

For each quasar in BOSS, DR9Q has 131 columns of data which has been collected on the object, ranging from simple identifying information to spectroscopic parameters derived for the BOSS spectra to data collected in non-optical bands by other surveys. Much of this data is taken directly from the BOSS pipeline, but additional data analysis is done in many places to improve on spectroscopic fits.

As our project was designed to analyze quasars which possess particular spectroscopic properties (namely, large FWHM and low continua), we were interested in having easy access to spectroscopic parameters on various important emission features. DR9Q contains calculations of FWHM, amplitude, and equivalent width for CIV as well as for two other emission lines, CIII] and MgII. However, rather than fitting the lines individually to Gaussian profiles as is performed by the BOSS pipeline (Bolton et al. 2012), Pâris et al. used a method of Principal Component Analysis (PCA) to model the lines. Their method involved taking a "training set" of quasar spectra which were believed to already be well parametrized and using them to form an eigenbasis, such that each newly analyzed quasar spectrum is fit to a linear combination of the spectra in the training set.

In the DR9Q release paper, Pâris et al. show that the quasar redshift derived through this

[4]The Space Telescope Science Institute has a number of informative introductions and tutorials to FITS files and PyFITS. See `http://www.stsci.edu/institute/software_hardware/pyfits`.

method matches the BOSS pipeline redshift closely and suggest that this method offers an improved measurement of the redshift (Pâris et al. 2012, § 3). However, they do not explicitly compare the measurement of emission line EW or FWHM from their analysis to those measurements generated by the BOSS pipeline. In order to determine whether we would rely upon the pipeline or the DR9Q values in deriving a quasar sample, we decided to compare the line parameters from the two sources.

### 3.2. Creation of the spData catalog

Searching repeatedly for pipeline data on the entire population of BOSS quasars is highly inefficient when the data is spread amongst hundreds of files for different plates and MJDs (one of the original reasons to produce the DR9Q catalog). To do a side-by-side comparison of the BOSS pipeline and DR9Q parameters, we needed a central catalog of information on all quasars, similar to DR9Q but containing instead only values generated by the pipeline. Using DR9Q as a source for the plates, fibers, and MJDs of all quasars in BOSS, we created our own FITS catalog of pipeline data by compiling data for all 87,822 quasars from the relevant spPlate, spZbest, and spZline files (see Appendix B). In keeping with the pipeline naming style, this catalog was stored in the file "spData.FITS", and will hereafter be referred to as *spData*. In order to optimize comparison of the two catalogs, the order of quasars in the spData data table was chosen to match DR9Q, so that columns from each file could be directly compared.

### 3.3. Comparison of CIV FWHM

The most important parameter which we wished to compare between DR9Q and spData was the measured width of the CIV line. CIV and Ly$\alpha$ are usually the two strongest emission lines observed in the optical bands for quasars at the high redshifts which BOSS probes ($z \gtrsim 2.0$). Ly$\alpha$ can be easily absorbed away by intervening neutral hydrogen, which, when at lower redshifts, may truncate the blue-edge of the emission line. This effect makes it quite difficult to accurately measure the width of the Ly$\alpha$ line, hence our choice to base our analysis on CIV.

The simplest first step was to plot the widths from the two methods against one another. Fig. 2 shows the results of this analysis. The plotted quasars are those which show CIV signal-to-noise ratio (S/N) of greater than 10, to remove noisy quasars from the analysis. S/N was calculated by taking the ratio of the calculated area of the emission line to the error in the same measurement (from the BOSS pipeline).

Interestingly, and unlike the measurement of redshift, the CIV FWHM values derived from the two methods are clearly not consistent. For all quasars measured to have FWHM $\lesssim$ 2000 km s$^{-1}$ from the pipeline (including the Type II candidate sample from Alexandroff 2012), the PCA method either overstates the FWHM or does not match the CIV line at all (FWHM = 0). At higher

spData velocities, the PCA method derives a lower value than the pipeline in most cases.

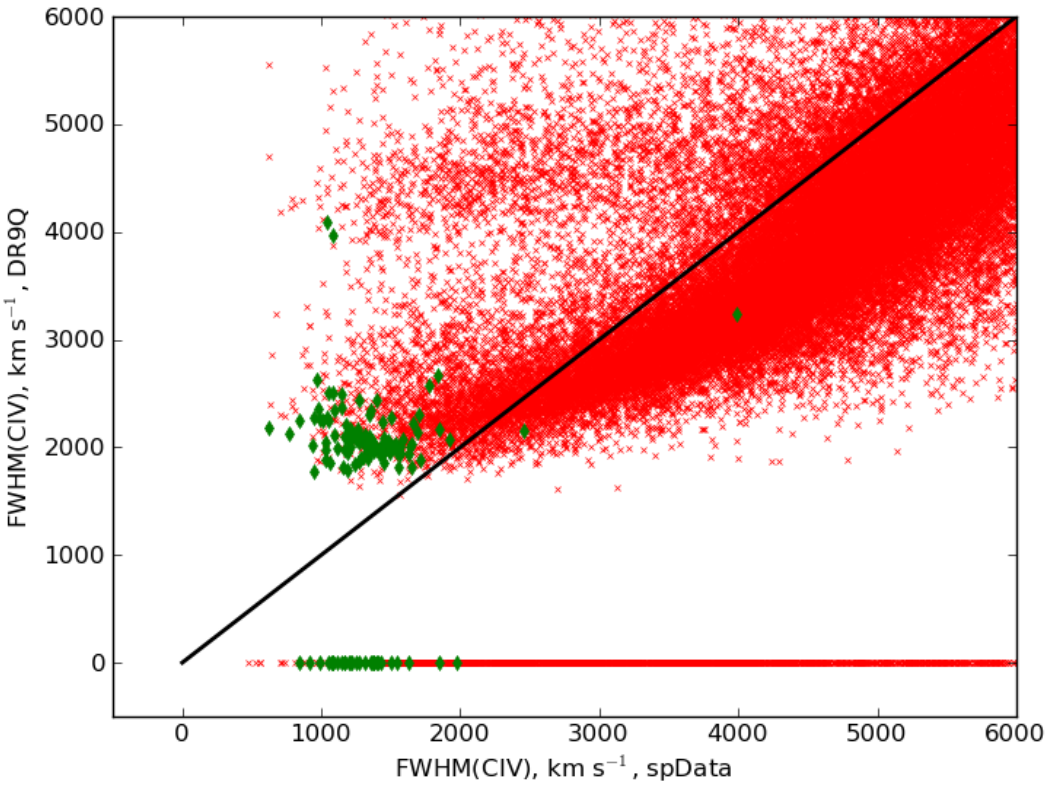


Fig. 2.— Comparison of the CIV FWHM inferred from the two different sources, the BOSS pipeline (catalog spData) and Pâris et al. (2012) (catalog DR9Q). Objects shown are those with CIV signal-to-noise ratio above 10, determined by the ratio of the CIV emission line area (from spData) divided by the error in the line area. Objects represented by green diamonds are candidate Type II quasars from Alexandroff 2012. It should be noted that, while Pâris et al. selected quasars with pipeline FWHM $\gtrsim$ 500 km s$^{-1}$ for their catalog, their PCA results are bereft of any quasars with FWHM $\lesssim$ 1500 km s$^{-1}$. Their results overestimate FWHM for *all* quasars with pipeline FWHM $\lesssim$ 2000 km s$^{-1}$, and fail to match (FWHM = 0) CIV emission for a large population of quasars where CIV is identified in the BOSS pipeline.

To make a judgment of the most reliable measurements, we visually inspected the CIV line fit for a number of quasars, including some of the Type II candidate sample from Alexandroff (2012). Because the PCA analysis does not assume a Gaussian profile, DR9Q does not give enough information to reconstruct the fit to the line itself, only the FWHM of the fit. Thus, for all models, a Gaussian profile with flux given by the BOSS pipeline was assumed, with the DR9Q model defined by its listed FWHM. An example of one of these comparisons is provided in Fig. 3.

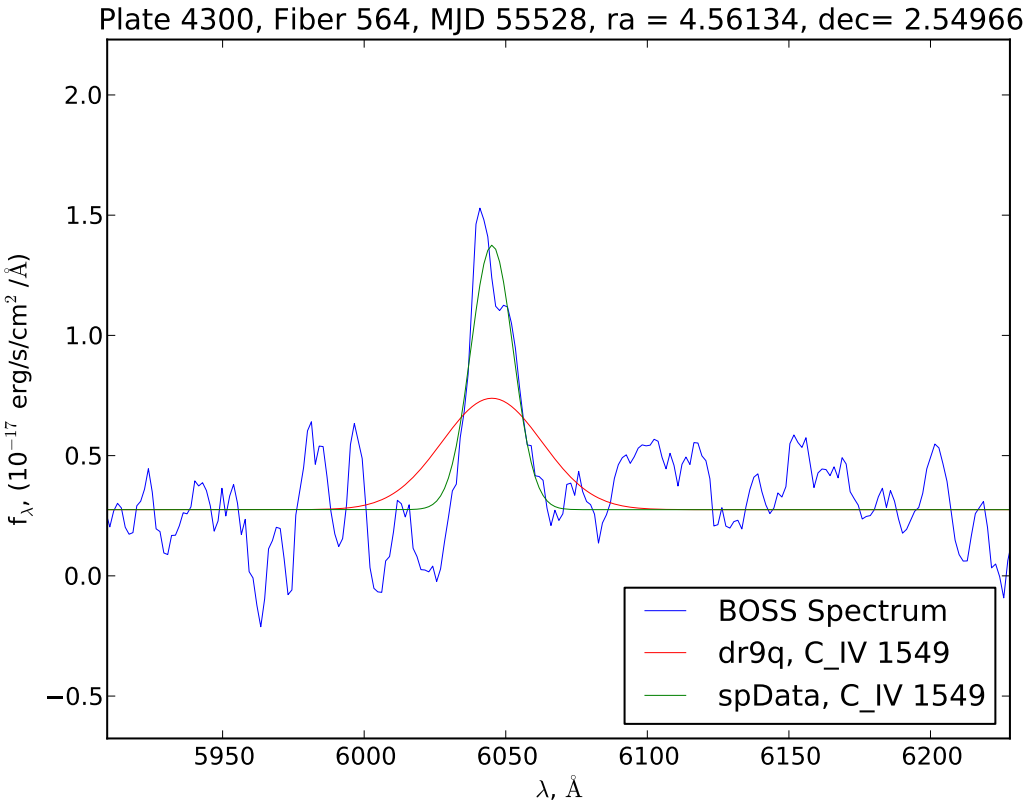


Fig. 3.— The BOSS spectrum of a quasar, focusing on the area around the CIV emission line. In green is the Gaussian fit parametrized by the BOSS pipeline (spData), while the red shows a similar fit to the data provided in the PCA fit by Pâris et al. (2012). Unfortunately, not all the data is available to provide the PCA-derived fit to the line, so we were forced to assume a Gaussian profile with the same area as given by the BOSS pipeline. This results in the DR9Q model appearing to have a lower peak amplitude than the actual emission line. It is recognized that this is an inconsistency on the part of this work, and the goodness-of-fit was not judged by this amplitude. Regardless, it can be easily inferred that Gaussian model with the FWHM given in DR9Q, even with the proper amplitude, would not fit the emission line properly, and the spData fit is more robust.

After visual analysis, it was decided that the spData provided a more reliable measure of the FWHM than DR9Q. While it is difficult to make definitive comparisons without the proper PCA fit, many visual inspections consistently showed the DR9Q FWHM to be a poor fit to the true width of the peak, particularly for the Type II candidate sample in Alexandroff (2012). For the remainder of the analysis, the spectral parameters derived from the BOSS pipeline will be utilized in place of the PCA fits from the DR9Q catalog. Despite the discrepancies in derived spectral

parameters, most of the data provided in DR9Q is incredibly useful, and we will rely on data such as IR magnitudes (see §5) provided in DR9Q throughout this work.

## 4. Identification of a Fat Quasar Sample in BOSS

### 4.1. Analysis of Known Objects

With the spData catalog line parameters, as well as supplemental data from DR9Q, we were prepared to begin looking for a population of fat quasars. The original objects identified by Alexandroff (2012) to possess broad emission lines and faint continua give us a starting point from which we can design a sample to look for similar objects. One parameter which was utilized was, necessarily, the previously discussed FWHM of the CIV line, as this will help identify objects with emission lines broad enough to suggest they are unobscured. Because we are simultaneously searching for objects with faint continua, we decided to also utilize the value of rest-frame equivalent width (REW), which is related to equivalent width (EW) simply by REW = EW / (1 + z). Because REW is a measure of the total luminosity of a line relative to the continuum, objects with broad spectral features (higher emission luminosity, for given amplitude) and faint continua would be expected to have high rest-frame equivalent width.

Fig. 4 shows the CIV REW and FWHM for quasars in BOSS with FWHM $\leq 6000\,\mathrm{km\,s^{-1}}$. As we predicted, the original fat quasar candidates[5] are characterized by unusually high REW. In order to search for similar objects, we thus defined a sample of all BOSS quasars with the properties:

$$\text{CIV REW} \geq 100\,\text{Å} \tag{5}$$

and

$$2000\,\mathrm{km\,s^{-1}} \leq \text{CIV FWHM} \leq 5000\,\mathrm{km\,s^{-1}}. \tag{6}$$

The sample with these ranges yielded a total of 285 quasars. We additionally applied a cut of CIV S/N $\geq 10$ (i.e. flux in CIV divided by the error), leaving us with a sample of 235 potential broad-emission-line, faint-continuum quasars.

### 4.2. Visual Inspection of the Sample

The spectrum of each of the 235 potential fat quasars in our sample was then individually inspected. The first criterion for which we were looking, broad emission lines, was checked by

[5]Only 3 fat candidates appear in the figure because one of them was not identified by the DR9Q catalog, and so was not included with our spData catalog upon its creation.

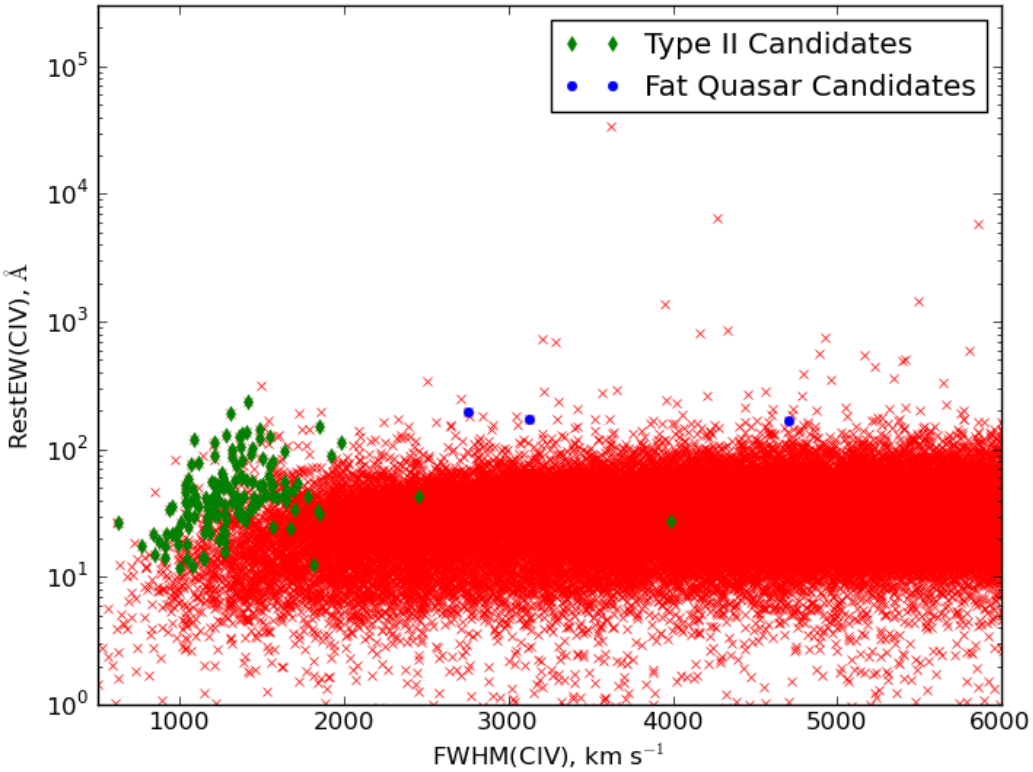


Fig. 4.— The distribution of REW versus FWHM for the CIV line of BOSS quasars with FWHM $\leq$ 6000 km s$^{-1}$. Objects represented by green diamonds are candidate Type II quasars identified in Alexandroff (2012), while blue circles represent the fat quasar candidates identified in the same work. These two populations, which are defined by faint continua, are predictably characterized by REW higher than average for objects with similar FWHM. All of the candidate fat quasars have REW $\geq$ 100 Å, and 2000 km s$^{-1}$ $\geq$ FWHM $\geq$ 5000 km s$^{-1}$, ranges which were used to select our fat quasar candidate sample. The objects with REW $\geq$ 1000 Å are outliers and are removed when we apply a cut of S/N $>$ 10 (see text).

visually inspecting the CIV and Ly$\alpha$ line profiles and confirming that they are matched well by the broad-FWHM fit provided by the BOSS spectrum. An example spectrum of one of the objects in the sample is shown in Fig. 5. For a few objects, there was sufficient noise in both emission lines that we could not confirm the measurement of a broad line width. In these cases, the quasar was marked for removal from the sample. However, possibly due to our cut of S/N $\geq$ 10, only three quasars were found which warranted removal for this reason. All three were quasars with z $<$ 2.0, such that Ly$\alpha$ was not in the SDSS range of detection, and the CIV line was too noisy to justify acceptance. Additionally, we inspected the entire spectrum of each quasar for evidence of a strong

or blueward-sloping continuum, which would violate the second criterion for admittance into the sample: a flat, faint continuum. Seven quasars were identified with such continua features, and were removed from the sample.

In total, fifteen quasars were found with traits which warranted removal from the sample. In addition to the seven already mentioned with strong continua and the three low-z quasars with noisy CIV lines, five other quasars were removed which were clearly Broad Absorption Line (BAL) quasars, due to strong absorption features to the blue end of all major spectral lines. Our final sample is thus comprised of 220 quasars whose spectra conform to the general character of fat quasars: broad emission lines but faint, flat continua. Fig. 6 shows an averaged spectrum of all 220 objects in the sample, emphasizing that the population as a whole has faint continua and broad emission lines.

Throughout the inspection, we kept a continual record of several other common traits, such as extremely strong NV emission lines or distinctive self-absorption features within the lines (noticed to various extents in most of the original four objects). Each trait was given a signifying key letter, and all of the letters which apply to a given object are combined into a *flag* of $\sim$ 1-4 keys. A guide to all keys used in the flags and a table of data on all objects in the final sample are included at the end of this work in Appendix A. Example spectra of some of the objects in the sample are also included, as well as a brief table of the 15 objects removed from the initial sample of 235.

## 5. Optical and Infrared Properties of the Fat Quasar Sample

Through our visual inspection, we confirmed that the 220 objects in our sample possess both broad emission lines (indicative of unobscured, Type I quasars) and faint, flat continua (indicative of obscured, Type II quasars). Another characteristic indicative of obscured quasars are very red colors, particularly when including photometry from the IR (where obscuring dust re-radiates a large fraction of absorbed UV light). In order to classify our sample of fat quasars as a distinct population, we also studied their optical and IR colors.

Of the 220 objects in our final sample, 37 have been detected in the infrared by the Wide-field Infrared Survey Explorer (WISE), a space telescope operated by NASA which operates four detectors in the mid-infrared. The four bands are known as W1, W2, W3, and W4, and are centered on 3.4, 4.6, 12, and 22 microns respectively (Wright et al. 2010). The DR9Q catalog includes the magnitude and error in the four WISE bands for any quasars which have been detected in the infrared survey. All 37 objects were detected in W1, with fewer identified in each longer-wavelength band. Only 28 were detected in all four WISE bands.

To characterize any possible obscuration of the objects in our sample, we calculated various colors r-Wx for the quasars, where r is the magnitude of the quasar in the SDSS optical r band ($\sim$6000 Å) and Wx represents one of the four WISE band magnitudes. In order to compare our sample to the population of faint BOSS quasars as a whole, we created a second sample of BOSS

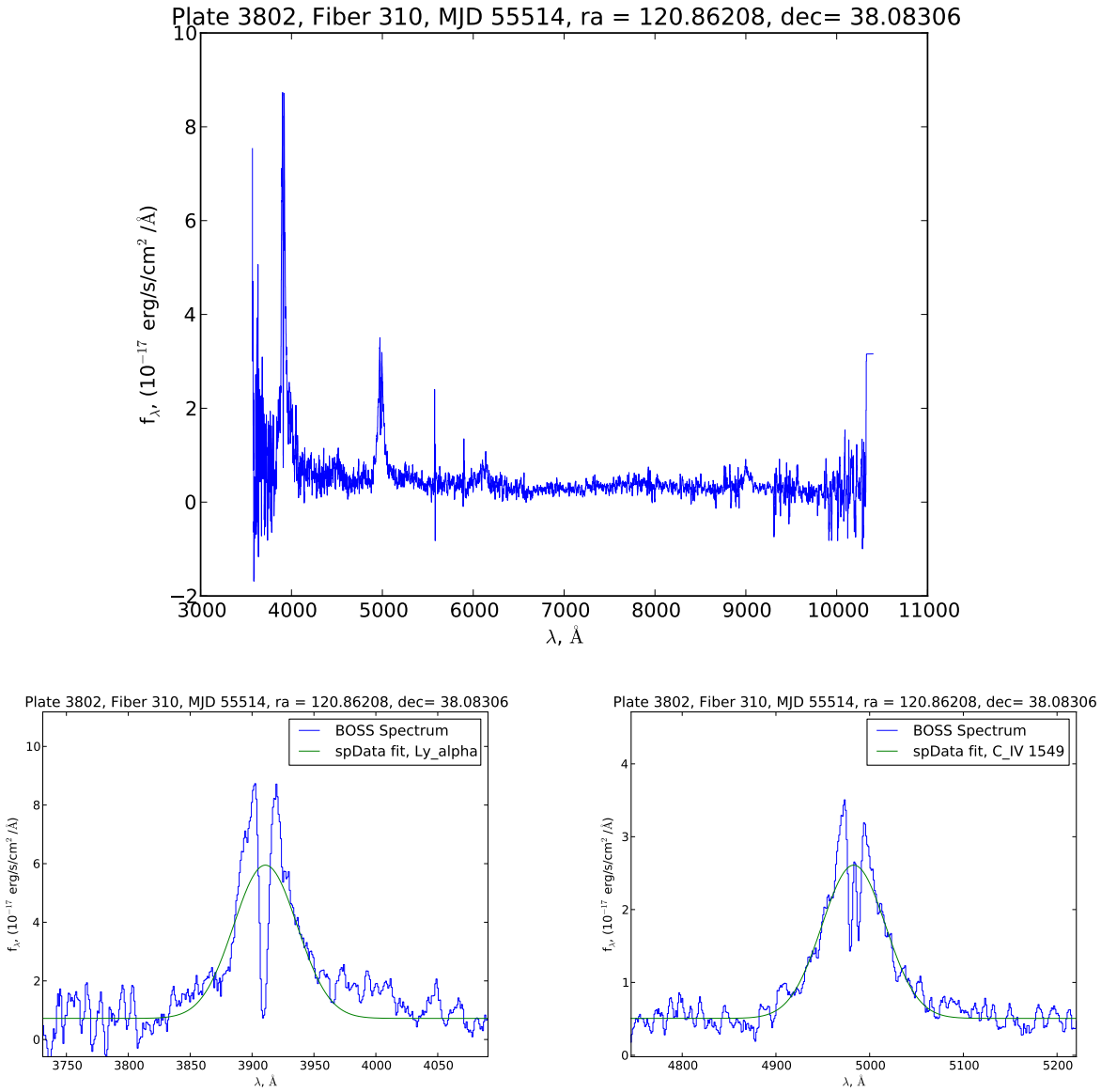


Fig. 5.— The spectrum of a candidate fat quasar identified in our sample. The redshift of the object is z = 2.216. *Upper*: The continuum of the quasar appears faint and flat, indicative of an obscured, Type II quasar. *Lower*: The Ly$\alpha$ (*left*) and CIV (*right*) lines are quite broad, with FWHM of 4640 and 4810 km s$^{-1}$ respectively, indicative of an unobscured, Type I quasar. The lines additionally show strong self-absorption. This quasar was given the flag "bS" (please see Appendix A.2)

.

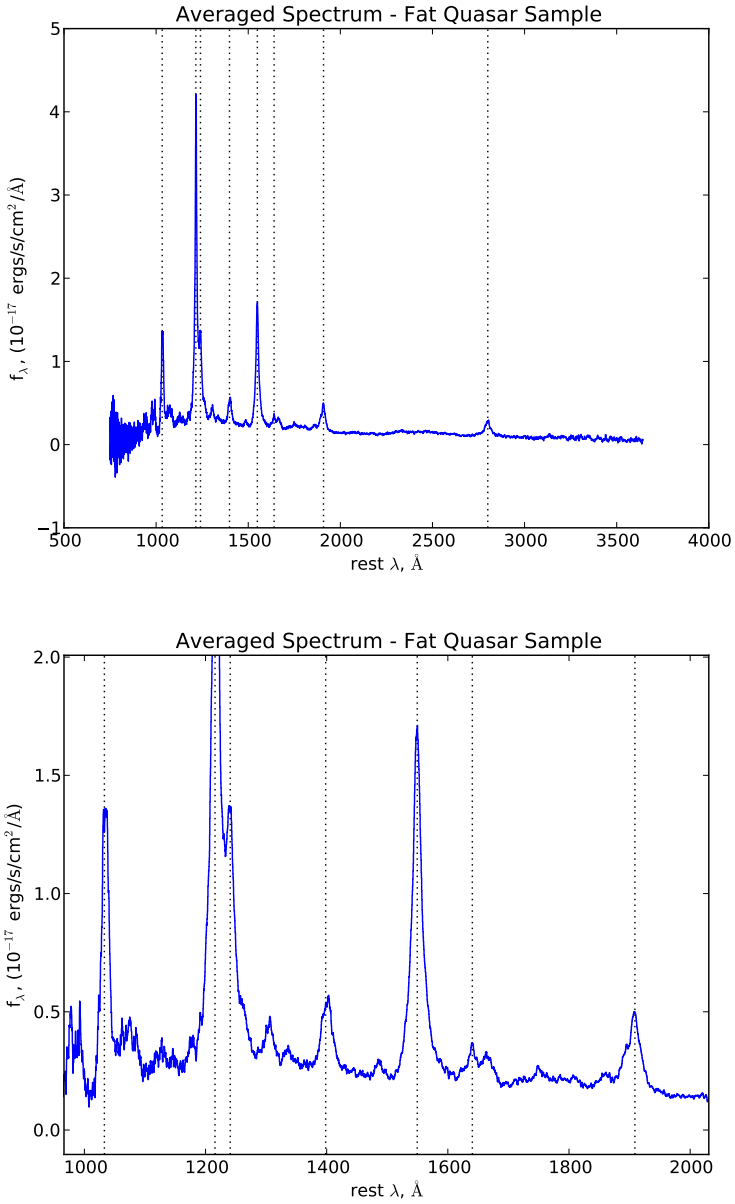


Fig. 6.— An averaged spectrum of all 220 quasars in our fat quasar sample. *Upper*: The entire spectrum, plotted over rest-frame wavelength. Note the faint, flat continuum throughout the spectrum, indicative of obscured Type II quasars. Identified spectral lines are, from left to right: Ly$\beta$, Ly$\alpha$, NV, SiIV + OIV] (a combined line), CIV, HeII, CIII], and MgII. *Lower*: A selected range of the same averaged spectrum. Identified spectral lines are, from left to right, same as above, with the exception of MgII (out of the frame). Note the very broad emission lines, indicative of unobscured Type I quasars.

quasars with faint r-band magnitudes. Because our fat quasar sample selected for objects with faint continua in the optical, their colors r-Wx are predisposed to be redder than the average BOSS quasar, even for similar Wx magnitudes. To control for this effect, our second sample contained all BOSS quasars with r-band magnitudes similar to those of our sample (and which were not already in our fat quasar sample). Fig. 7 shows the distribution of r-band magnitudes for the BOSS population as a whole, our fat quasar sample, and BOSS quasars with S/N $\geq$ 10. As expected, our sample is much fainter in r, peaking around 22, as opposed to 20.5 for the whole BOSS population. We selected BOSS quasars with r $\geq$ 21 to create our secondary comparison sample with similar r-band magnitudes. Table 1 shows the fraction of detections in the various WISE bands for the BOSS quasars as a whole, for those with r $\geq$ 21, and for our sample of fat quasars. The WISE detection rate for the fat quasar sample is comparable to the BOSS quasars with r $\geq$ 21 and is higher in the W4 band. To analyze these values more robustly will require a more carefully derived control sample (see §6.1).

| | All BOSS quasars | r $\geq$ 21 | fat quasars |
|---|---|---|---|
| W1 | .52 | .20 | .17 |
| W2 | .52 | .20 | .16 |
| W3 | .51 | .19 | .16 |
| W4 | .37 | .09 | .13 |

Table 1: The fraction of quasars detected in each WISE band. Note that the fat-quasar sample has a particularly high detection rate in the W4 band compared to all other BOSS quasars with r $\geq$ 21.

From these two samples, we calculated the r-Wx colors for all objects which were detected in each W band. The definition of the magnitude system leads to very red objects (brighter in IR than optical) having more highly positive r-Wx colors than blue objects. While this method will preferentially select those objects which are most luminous in the IR (i. e. detected in WISE), and thus more likely to be obscured, this W-selection bias is balanced by applying it to both samples. As stated above, the fat quasar sample with these W-detection cuts contains between 37 and 28 quasars, while the r $\geq$ 21 BOSS sample contains between 6500 and 2800 quasars detected in WISE.

Fig. 8 shows the color distributions for all BOSS quasars detected in WISE, the r $\geq$ 21 sample, and the fat quasar sample. These results show that, particularly in r-W3 and r-W4 colors, our fat quasar sample is quite redder on average than the BOSS sample as a whole. The r $\geq$ 21 sample appears to have similar median colors to the fat quasar sample, but a much narrower distribution. Small number statistics for the fat quasar sample could possibly be to blame for this effect, but to confirm or deny this, we applied a two-sample Kolmogorov-Smirnov (KS) test to the two samples. A two-sample KS test analyzes the probability distributions of two given samples of data, giving a statistical probability that two distributions which were drawn out of the same continuous distribution would have differences of the order seen between the two samples. If this probability (p) is less than some pre-determined cutoff (often 0.05 or 0.01) then it is often

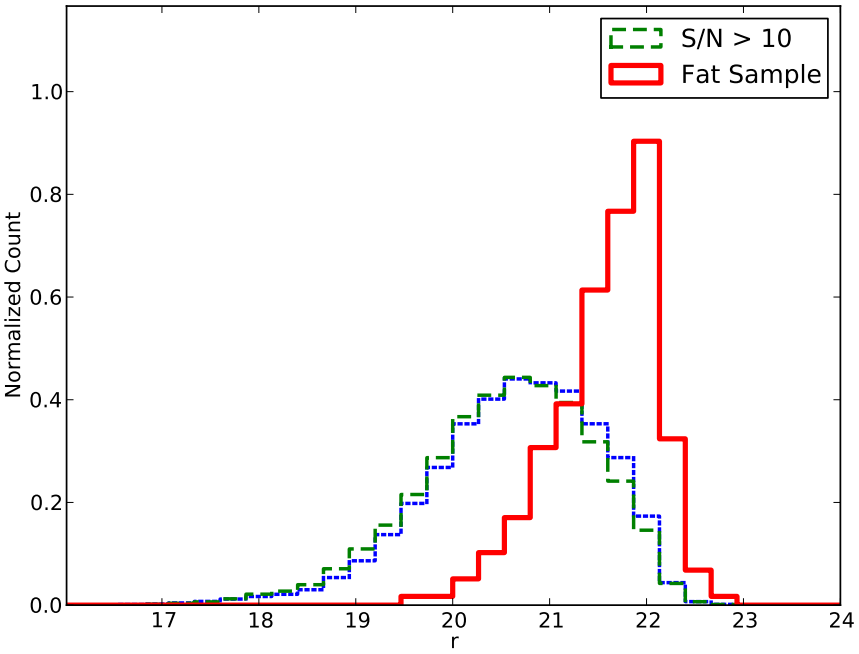


Fig. 7.— The distribution of r-band magnitudes for different samples of BOSS quasars. The blue-dotted histogram shows the entire sample of BOSS quasars released in DR9, and the green-dashed histogram represents those BOSS quasars with S/N in CIV $\geq$ 10. The red histogram is our sample of 220 fat quasars, which as a population is quite obviously dimmer in r. This was selected for through our selection of CIV REW $\geq$ 100Å (i.e. low continua). In creating a sample of all BOSS quasar with similar r-band magnitudes to our fat quasar sample (see text) we applied a magnitude cut of r $\geq$ 21, matching the majority of the fat quasar sample.

interpreted that the two samples do not represent random samples from the same population.[6] The two-sample KS test p-values calculated between the fat quasar sample and the two others (BOSS as a whole, and those quasars with r $\geq$ 21) is shown in Table 2.

The very low p-values for these tests support our observations from Fig. 8, that the r-Wx color distribution for fat quasars is redder than for the BOSS population as a whole, and statistically different than for the population of all BOSS quasars with faint r-band magnitudes. We conclude from these results that, due to their IR luminosity and colors (particularly in W3 and W4), the fat quasars do not simply have faint rest-frame UV (observed optical) continua, but are at least

[6]This interpretation is not completely valid, as the KS-test does NOT test the probability that the two samples come from the same population, but the probability of drawing similar samples IF they did come from the same population. This is a subtle point and not to be overlooked in general.

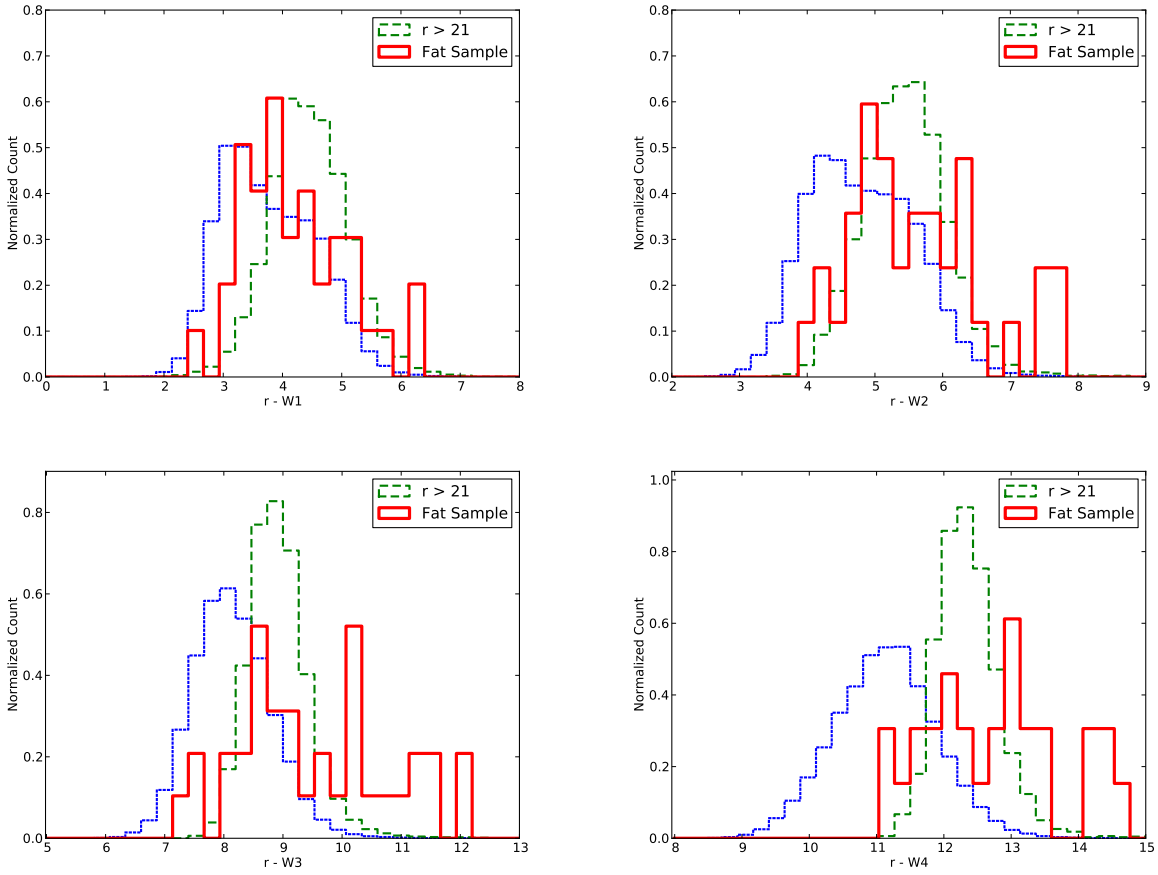


Fig. 8.— The distribution of r-W colors for those quasars with detections by WISE. The blue dotted histograms represent all BOSS quasars detected in WISE which are not in our fat quasar sample, the green dashed histograms represent those BOSS quasars with r $\geq$ 21, and the red solid histograms, our fat quasar sample. The distribution of IR colors for the fat quasar population is distinctly different from the overall BOSS population, particularly for the redder r-W3 and r-W4 colors. While it may suffer from small sample sizes, it can be seen to have a wider distribution than the r $\geq$ 21 sample. Notice, in particular, an apparent excess of very red objects in the fat quasar sample (r-W3 $>$ 10 or r-W4 $>$ 13). A Kolmogorov-Smirnov test confirms these conclusions (see text).

partially obscured, resulting in their flat, faint rest-frame UV continua and bright IR emission. This increases our curiosity as to why these objects have such broad emission lines, in disagreement with the standard unification picture of obscured and unobscured quasars.

| | fat quasars vs. all BOSS | fat quasars vs. r $\geq$ 21 |
|---|---|---|
| r-W1 | p = 0.0182 | p = 0.00791 |
| r-W2 | p = 2.48x10$^{-4}$ | p = 0.110 |
| r-W3 | p = 4.40x10$^{-11}$ | p = 2.68x10$^{-5}$ |
| r-W4 | p = 4.19x10$^{-12}$ | p = 3.20x10$^{-4}$ |

Table 2: Two-Sample KS Test p-values for distributions of r-Wx colors. These results indicate that the fat quasar sample colors are not a random sampling from the larger BOSS population and may instead represent a unique population of objects.

## 6. Conclusions

We have identified a sample of 220 "fat quasars" which cannot be simply classified into the framework of obscured/unobscured which describes the current understanding of quasar properties. This sample was designed to identify candidates to match an initial sample of four interesting quasars found in Alexandroff (2012). The sample was selected by their CIV emission line properties: REW $\geq$ 100 Å, 2000 km s$^{-1}$ $\leq$ FWHM $\leq$ 5000 km s$^{-1}$, and a S/N ratio in CIV $\geq$ 10.

These spectral properties were generated by the BOSS pipeline, as our analysis indicated that the values obtained through the PCA modeling of Pâris et al.'s DR9Q catalog were less accurate measures of the true width of the emission lines. DR9Q was nevertheless used as a catalog of which BOSS objects were quasars, as well as other information such as the WISE band magnitudes for various quasars.

These quasars exhibit some obscured properties, namely faint, flat rest-frame UV continua. The fraction ($\sim$15%) which have detections in WISE have relatively bright IR luminosities as well. Yet they also exhibit broad emission lines (over 4000 km s$^{-1}$ in many cases) which would otherwise classify them into the Type I, unobscured category. It is not apparent what might be causing these objects to possess characteristics of both types.

### 6.1. Future Work

In order to identify more of these interesting fat quasars, future samples should explore higher FWHM ranges ($>$ 5000 km s$^{-1}$). If objects similar to our fat quasars are found to have such extremely broad emission lines as well as extinguished UV spectra, it will pose further challenges to the current dusty-torus unification model.

Infrared measurements of our sample have been useful in identifying the fat quasars as likely extinguished by dust, suggesting the presence of obscuring material near the central engines. Future work would also benefit from increased observations of these fat quasars in the IR, which can further constrain the level of obscuration around these objects.

Additionally, a more highly-refined control sample should be utilized, to better reproduce the r-band magnitude distribution of our sample. One way to create such a sample would be to randomly select multiple quasars from the overall BOSS population which match closely the magnitude of each of the 220 quasars in the fat sample.

Coming in July 2013, the release of SDSS DR10 will more than double the number of BOSS quasar spectra available for study (Strauss, Michael; personal correspondence). We believe that the continuation of this research with the data available from SDSS DR10 would greatly improve our ability to identify and characterize the fat quasar population.

These fat quasars provide interesting questions which may not be easily answered with our current understanding of quasar properties. These objects may, for instance, represent borderline cases, where our line-of-sight intersects only glancingly with the dusty torus, allowing us to view the broad-line region, but still resulting in significant UV extinction into the IR. In other models such as the evolving dust layer described by Hopkins et al. (2006), this population of fat quasars may represent an intermediate stage of quasar development, while the quasar is beginning to blow away its dust coverings. Many questions remain unanswered about the true nature of quasars, and future observations, analysis, and theories will surely one day lead us to a more complete understanding of these fascinating objects.

Incredible thanks go to my adviser, Prof. Michael Strauss. His expertise and knowledge were essential to the completion of this project, as were his patience and guidance to my own improvement as a scientist. He has been an irreplaceable resource and partner, and the ability to produce a single result which he was unable to explain was a fantastic reward to the semester.

Additional thanks to Rachael Alexandroff for her wonderful Senior Thesis, upon which this work originates and upon which I relied heavily to solidify my understanding of quasar science as I began the project.

This paper represents my own work in accordance with University regulations.

# A. Fat Quasar Sample

This appendix holds more detailed information on the identified sample of fat quasars.

## A.1. Flag Keys Used

Table 3:: Descriptions of the various flag key letters used in visual analysis of the fat quasar sample.

| Flag Key | Description |
|---|---|
| 1 | Ly$\alpha$ fit parameters (usually continuum level) miscalculated by pipeline |
| a | Evidence of BAL-type absorption |
| B | Blue sloping continuum |
| E | Instrumental error present in spectrum |
| F | Evidence of significant Ly$\alpha$ forest absorption (no absorption in CIV) |
| H | High (bright) continuum level |
| K | Sky line prominent near CIV or Ly$\alpha$ |
| L | Ly$\alpha$ line is not well fit by a Gaussian |
| N | NV line emission of comparable strength to Ly$\alpha$ (often absorbs away Ly$\alpha$) |
| n | NV line faint, but gives Ly$\alpha$ abnormally broad appearance. |
| P | Poor or noisy data |
| V | Significant difference in Ly$\alpha$ and CIV velocity (FWHM) |
| S | Strong self-absorption found in both Ly$\alpha$ and CIV lines |
| s | Possible self-absorption found in both Ly$\alpha$ and CIV, or strong self-absorption found in one. |
| X | Removed from sample |
| Z | Quasar Redshift too low (z $\lesssim$ 2.0) to observe Ly$\alpha$. |

### A.2. Objects in the Final Sample

Table 4:: Table of 220 fat quasars, selected and confirmed to have broad emission lines and faint continua. All line values are for CIV. S/N represents line flux divided by error.

| Plate | Fiber | MJD | RA ° | Dec ° | z | FWHM km s$^{-1}$ | REW Å | S/N | Flag |
|---|---|---|---|---|---|---|---|---|---|
| 4219 | 800 | 55480 | 5.42454 | 0.91888 | 2.290 | 3270 | 110 | 53 | - |
| 4220 | 789 | 55447 | 7.15032 | 1.12246 | 2.817 | 4880 | 124 | 24 | F |
| 4303 | 300 | 55508 | 9.09456 | 3.68680 | 1.584 | 3400 | 147 | 36 | Z |
| 3587 | 274 | 55182 | 9.10194 | -0.40812 | 2.311 | 4570 | 109 | 36 | B |
| 4304 | 828 | 55506 | 10.50069 | 3.03177 | 2.171 | 4580 | 135 | 36 | - |
| 4224 | 438 | 55481 | 12.92588 | -0.25821 | 2.740 | 4930 | 107 | 14 | - |
| 4307 | 282 | 55531 | 13.95887 | 2.60952 | 2.381 | 3940 | 118 | 22 | - |
| 4224 | 878 | 55481 | 14.17991 | 0.89310 | 2.554 | 4590 | 134 | 48 | - |
| 4551 | 310 | 55569 | 17.20032 | 9.28719 | 1.694 | 4790 | 103 | 15 | Z |
| 4227 | 974 | 55481 | 19.64042 | 0.38690 | 2.380 | 4250 | 153 | 13 | V |
| 4228 | 330 | 55484 | 20.08619 | -1.00746 | 2.469 | 3320 | 131 | 11 | - |
| 4352 | 634 | 55533 | 20.81316 | -1.41339 | 4.066 | 2180 | 120 | 27 | - |
| 4661 | 476 | 55614 | 23.13772 | 13.46562 | 3.219 | 4770 | 144 | 12 | S |
| 4230 | 255 | 55483 | 23.74214 | -0.98193 | 2.401 | 3620 | 111 | 46 |  |
| 4350 | 370 | 55556 | 25.29640 | -3.31460 | 2.538 | 3190 | 106 | 62 | N |
| 4275 | 970 | 55501 | 26.20996 | 2.59530 | 1.945 | 3860 | 159 | 45 | Z |
| 4403 | 357 | 55536 | 27.34320 | 5.93152 | 2.342 | 2980 | 101 | 83 |  |
| 4233 | 48 | 55449 | 29.78824 | -0.60037 | 2.382 | 4870 | 151 | 18 | S |
| 4233 | 34 | 55449 | 29.88574 | -0.15321 | 2.657 | 4590 | 111 | 15 | NK |
| 4234 | 910 | 55478 | 31.16886 | 1.24896 | 2.633 | 4730 | 144 | 11 | K |
| 4236 | 146 | 55479 | 34.28322 | -0.60507 | 3.864 | 3390 | 100 | 35 | 1La |
| 4400 | 940 | 55509 | 34.84787 | 6.53263 | 2.298 | 3420 | 119 | 30 | - |
| 4267 | 56 | 55484 | 35.21715 | 1.61976 | 3.127 | 3120 | 173 | 24 | NF |
| 3615 | 580 | 55179 | 36.25021 | 0.23462 | 3.003 | 4410 | 150 | 68 | LNa |
| 4260 | 174 | 55478 | 39.51083 | 3.27615 | 2.445 | 4780 | 104 | 32 | B |
| 4240 | 842 | 55455 | 40.93643 | 0.58977 | 3.029 | 2290 | 109 | 43 | F |
| 4240 | 918 | 55455 | 41.31167 | 0.65649 | 2.451 | 4070 | 146 | 20 | - |
| 4444 | 910 | 55538 | 113.77811 | 33.53453 | 2.331 | 4330 | 109 | 29 | 1F |
| 3664 | 428 | 55245 | 113.79201 | 39.54262 | 2.231 | 4530 | 118 | 25 | - |
| 4470 | 516 | 55587 | 113.88824 | 23.70564 | 3.301 | 2510 | 341 | 26 | - |
| 3664 | 620 | 55245 | 114.10280 | 39.96419 | 2.436 | 3650 | 105 | 36 | - |
| 3662 | 840 | 55182 | 114.44241 | 38.07975 | 2.577 | 4520 | 107 | 27 | 1K |

Table 4:: Table of 220 fat quasars, selected and confirmed to have broad emission lines and faint continua. All line values are for CIV. S/N represents line flux divided by error.

| Plate | Fiber | MJD | RA ° | Dec ° | z | FWHM km s$^{-1}$ | REW Å | S/N | Flag |
|---|---|---|---|---|---|---|---|---|---|
| 4448 | 408 | 55538 | 115.27448 | 29.81936 | 2.829 | 3950 | 120 | 14 | - |
| 4497 | 324 | 55564 | 115.81284 | 14.64797 | 2.176 | 4530 | 100 | 37 | - |
| 3669 | 218 | 55481 | 116.03021 | 42.62383 | 2.429 | 4720 | 115 | 32 | 1S |
| 3668 | 910 | 55478 | 117.19673 | 50.22241 | 2.455 | 4410 | 109 | 68 | - |
| 4497 | 26 | 55564 | 117.23396 | 15.03925 | 2.429 | 3150 | 104 | 27 | 1 |
| 3668 | 80 | 55478 | 117.25257 | 49.16201 | 1.595 | 4380 | 101 | 26 | Z |
| 4482 | 522 | 55617 | 117.90008 | 21.13137 | 2.247 | 2920 | 104 | 14 | V |
| 3676 | 934 | 55186 | 118.86570 | 43.80194 | 1.545 | 3090 | 120 | 11 | Z |
| 3680 | 692 | 55210 | 119.17894 | 41.55883 | 2.931 | 3540 | 121 | 19 | SNFa |
| 4494 | 670 | 55569 | 119.99646 | 17.41821 | 2.501 | 4060 | 116 | 37 | - |
| 3802 | 310 | 55514 | 120.86208 | 38.08306 | 2.216 | 4810 | 110 | 30 | S |
| 3755 | 184 | 55504 | 121.08484 | 30.42969 | 2.273 | 2320 | 123 | 45 | - |
| 3681 | 76 | 55243 | 121.10728 | 47.03313 | 2.753 | 2650 | 155 | 46 | Na |
| 3701 | 606 | 55540 | 122.15239 | 54.38480 | 2.329 | 4930 | 109 | 34 | - |
| 4509 | 540 | 55574 | 122.45079 | 11.19013 | 2.380 | 4080 | 101 | 15 | 1 |
| 4481 | 900 | 55630 | 122.89225 | 21.38427 | 2.545 | 4470 | 150 | 12 | 1S |
| 3701 | 698 | 55540 | 123.03959 | 54.10210 | 1.555 | 2370 | 126 | 24 | Z |
| 4450 | 532 | 55540 | 123.95814 | 29.41109 | 2.190 | 4680 | 111 | 12 | - |
| 3693 | 615 | 55208 | 124.24938 | 48.50185 | 2.502 | 3910 | 103 | 12 | - |
| 3693 | 636 | 55208 | 124.49411 | 49.29435 | 2.348 | 4690 | 110 | 20 | - |
| 4509 | 68 | 55574 | 124.51590 | 10.60115 | 2.399 | 4800 | 157 | 14 | - |
| 3808 | 524 | 55513 | 125.67118 | 41.56207 | 2.513 | 4810 | 115 | 36 | K |
| 3761 | 648 | 55272 | 126.07735 | 39.90657 | 2.488 | 2090 | 107 | 58 | S |
| 4446 | 857 | 55589 | 126.10400 | 32.70193 | 2.490 | 4490 | 110 | 39 | 1 |
| 3696 | 572 | 55277 | 126.32997 | 48.97503 | 2.203 | 4020 | 131 | 20 | - |
| 3807 | 64 | 55511 | 126.38524 | 42.67585 | 2.746 | 4230 | 133 | 32 | - |
| 3690 | 118 | 55182 | 126.51525 | 52.79459 | 1.526 | 3040 | 180 | 27 | Z |
| 4764 | 530 | 55646 | 126.72262 | 5.71315 | 2.573 | 2560 | 163 | 90 | NF |
| 3762 | 644 | 55507 | 126.81461 | 36.58839 | 1.633 | 3690 | 102 | 27 | Z |
| 4496 | 894 | 55544 | 128.00085 | 16.25010 | 2.425 | 4710 | 168 | 43 | SN |
| 4454 | 466 | 55536 | 128.27611 | 27.64591 | 3.253 | 2050 | 108 | 33 | FN |
| 4793 | 452 | 55648 | 128.63721 | -0.23731 | 2.351 | 4200 | 130 | 14 | P |
| 4794 | 260 | 55647 | 128.70203 | 1.98921 | 2.584 | 2750 | 197 | 41 | K |
| 4460 | 928 | 55533 | 129.29716 | 26.45725 | 2.409 | 4710 | 107 | 46 | - |

Table 4:: Table of 220 fat quasars, selected and confirmed to have broad emission lines and faint continua. All line values are for CIV. S/N represents line flux divided by error.

| Plate | Fiber | MJD | RA ° | Dec ° | z | FWHM km s$^{-1}$ | REW Å | S/N | Flag |
|---|---|---|---|---|---|---|---|---|---|
| 3763 | 986 | 55508 | 129.81360 | 38.35373 | 2.109 | 4700 | 134 | 11 | PS |
| 3809 | 84 | 55533 | 130.81435 | 2.51636 | 2.495 | 2870 | 102 | 34 | - |
| 3817 | 92 | 55277 | 136.79945 | 2.96961 | 2.372 | 3880 | 168 | 23 | S |
| 3820 | 580 | 55542 | 137.27290 | 4.45928 | 1.744 | 4820 | 163 | 19 | Z |
| 3780 | 796 | 55240 | 137.45000 | -0.96995 | 2.441 | 4550 | 111 | 24 | 1 |
| 4645 | 37 | 55623 | 138.05945 | 35.75141 | 2.051 | 4600 | 101 | 21 | - |
| 4576 | 520 | 55592 | 140.74638 | 36.23915 | 2.776 | 4500 | 119 | 14 | 1 |
| 3781 | 959 | 55243 | 142.30457 | -1.13130 | 2.214 | 4620 | 101 | 40 | B |
| 4575 | 468 | 55590 | 143.62161 | 35.71188 | 1.583 | 3830 | 101 | 30 | Z |
| 4742 | 915 | 55660 | 143.94739 | 3.00690 | 2.155 | 4130 | 109 | 29 | ZaL |
| 3826 | 724 | 55563 | 145.10658 | 0.56719 | 2.334 | 3120 | 114 | 87 | 1 |
| 3768 | 488 | 55564 | 147.32178 | -2.50125 | 2.290 | 4770 | 138 | 17 | - |
| 3768 | 644 | 55564 | 148.25816 | -0.55536 | 2.211 | 4680 | 103 | 31 | S |
| 4573 | 156 | 55587 | 148.58739 | 36.14446 | 2.581 | 4470 | 111 | 21 | KS |
| 4570 | 762 | 55623 | 149.21881 | 39.04298 | 3.128 | 4210 | 260 | 18 | NF |
| 4637 | 522 | 55616 | 149.60052 | 36.89147 | 2.415 | 4360 | 118 | 25 | - |
| 4693 | 476 | 55632 | 150.63802 | 44.26065 | 3.303 | 4440 | 211 | 34 | 1F |
| 4800 | 258 | 55674 | 150.81548 | 3.92245 | 2.253 | 4720 | 123 | 29 | - |
| 4874 | 28 | 55673 | 151.10040 | 6.37566 | 1.712 | 4200 | 102 | 24 | Z |
| 4693 | 626 | 55632 | 151.29196 | 45.55452 | 2.256 | 2840 | 104 | 18 | - |
| 3783 | 74 | 55246 | 151.39485 | -1.98790 | 2.185 | 3950 | 106 | 35 | - |
| 4875 | 158 | 55677 | 152.50443 | 6.56282 | 2.190 | 2250 | 112 | 47 | - |
| 4738 | 954 | 55650 | 153.22806 | 3.59685 | 3.154 | 3660 | 291 | 21 | S |
| 4564 | 510 | 55570 | 154.44698 | 35.96419 | 2.439 | 4090 | 138 | 16 | - |
| 4802 | 426 | 55652 | 154.85809 | 3.76025 | 2.213 | 4680 | 149 | 75 | - |
| 4876 | 916 | 55679 | 155.02222 | 7.19740 | 2.615 | 4590 | 101 | 22 | KF |
| 4876 | 61 | 55679 | 155.43211 | 6.12489 | 2.442 | 4800 | 103 | 19 | - |
| 4851 | 566 | 55680 | 155.81526 | 7.08133 | 3.598 | 4800 | 104 | 90 | NaF |
| 4692 | 910 | 55644 | 155.95602 | 45.66397 | 2.246 | 4430 | 107 | 50 | S |
| 4632 | 698 | 55644 | 158.59109 | 42.44949 | 2.660 | 3810 | 141 | 18 | |
| 4691 | 200 | 55651 | 158.68553 | 44.55286 | 2.509 | 4150 | 160 | 21 | 1 |
| 4773 | 864 | 55648 | 160.85744 | 5.38858 | 2.591 | 4240 | 106 | 25 | KF |
| 4689 | 624 | 55656 | 163.43713 | 45.24839 | 2.150 | 3580 | 118 | 16 | 1 |
| 4621 | 146 | 55649 | 168.67538 | 38.85363 | 1.725 | 4700 | 103 | 23 | ZB |

Table 4:: Table of 220 fat quasars, selected and confirmed to have broad emission lines and faint continua. All line values are for CIV. S/N represents line flux divided by error.

| Plate | Fiber | MJD | RA ° | Dec ° | z | FWHM km s$^{-1}$ | REW Å | S/N | Flag |
|---|---|---|---|---|---|---|---|---|---|
| 3774 | 616 | 55244 | 170.05788 | -1.60348 | 1.563 | 3820 | 110 | 28 | ABa |
| 3838 | 998 | 55588 | 170.64696 | 0.12763 | 2.263 | 3640 | 136 | 13 | P |
| 4730 | 796 | 55630 | 171.81792 | 3.02173 | 2.430 | 4190 | 102 | 53 | SB |
| 4730 | 126 | 55630 | 172.29201 | 1.03033 | 2.325 | 2900 | 145 | 11 | - |
| 4648 | 720 | 55673 | 173.08235 | 38.64536 | 2.304 | 4630 | 108 | 21 | S |
| 4648 | 45 | 55673 | 174.52710 | 37.07217 | 2.104 | 4890 | 104 | 40 | - |
| 4765 | 288 | 55674 | 178.12074 | 3.70498 | 2.377 | 4600 | 138 | 35 | F |
| 3776 | 418 | 55209 | 178.81883 | -2.67889 | 2.576 | 2790 | 111 | 15 | 1K |
| 4652 | 872 | 55672 | 179.45483 | 38.93452 | 2.227 | 2390 | 151 | 13 | - |
| 4611 | 522 | 55603 | 180.36882 | 33.28742 | 2.188 | 4140 | 131 | 19 | - |
| 4611 | 610 | 55603 | 180.88318 | 33.12948 | 2.200 | 3810 | 108 | 13 | - |
| 4831 | 210 | 55679 | 181.76479 | 5.70991 | 2.316 | 4990 | 119 | 13 | - |
| 3845 | 801 | 55323 | 182.86130 | 0.74271 | 2.352 | 4600 | 185 | 12 | P |
| 4832 | 366 | 55680 | 184.06589 | 4.93221 | 2.329 | 3920 | 133 | 21 | - |
| 3777 | 318 | 55210 | 184.17804 | -2.11465 | 1.859 | 4030 | 140 | 24 | Z |
| 4750 | 724 | 55630 | 184.26961 | 2.57143 | 2.416 | 2760 | 182 | 57 | N |
| 3846 | 755 | 55327 | 184.67258 | 0.87855 | 2.322 | 4110 | 159 | 12 | P |
| 3777 | 996 | 55210 | 185.63525 | -1.74318 | 3.872 | 4560 | 152 | 28 | NaL1 |
| 3967 | 430 | 55704 | 185.71423 | 39.03363 | 3.880 | 4040 | 127 | 40 | F |
| 3847 | 778 | 55588 | 186.61446 | 0.42237 | 2.792 | 3720 | 112 | 25 | - |
| 3792 | 864 | 55212 | 187.54105 | -0.34172 | 2.131 | 4870 | 139 | 12 | P |
| 4833 | 60 | 55679 | 188.04437 | 5.24209 | 2.426 | 4130 | 114 | 21 | - |
| 3969 | 140 | 55307 | 190.08778 | 36.64904 | 2.895 | 4590 | 124 | 15 | - |
| 3970 | 130 | 55591 | 190.26697 | 38.71507 | 2.970 | 4970 | 110 | 22 | - |
| 3794 | 196 | 55241 | 194.41707 | -2.05486 | 2.239 | 4070 | 117 | 41 | - |
| 4005 | 888 | 55325 | 196.06259 | 2.42460 | 2.489 | 4910 | 104 | 19 | - |
| 3978 | 646 | 55330 | 196.25935 | 38.60144 | 2.328 | 3230 | 110 | 40 | S |
| 3977 | 910 | 55335 | 197.15565 | 36.15276 | 2.954 | 2890 | 103 | 15 | - |
| 4052 | 159 | 55600 | 197.27533 | 0.13604 | 2.302 | 3550 | 119 | 39 | 1 |
| 3977 | 937 | 55335 | 197.48724 | 35.66400 | 2.779 | 3420 | 208 | 12 | 1V |
| 4053 | 654 | 55591 | 197.64507 | -2.06383 | 2.494 | 3610 | 173 | 10 | - |
| 3981 | 346 | 55603 | 198.89987 | 38.07179 | 2.165 | 4750 | 107 | 32 | S |
| 4707 | 572 | 55653 | 199.69574 | 40.85974 | 2.517 | 4730 | 207 | 20 | 1 |
| 4049 | 584 | 55591 | 199.80469 | -1.21547 | 2.221 | 4050 | 103 | 29 | - |

Table 4:: Table of 220 fat quasars, selected and confirmed to have broad emission lines and faint continua. All line values are for CIV. S/N represents line flux divided by error.

| Plate | Fiber | MJD | RA ° | Dec ° | z | FWHM km s$^{-1}$ | REW Å | S/N | Flag |
|---|---|---|---|---|---|---|---|---|---|
| 4761 | 334 | 55633 | 200.21111 | 3.58170 | 2.584 | 3730 | 103 | 25 | KF |
| 4050 | 456 | 55599 | 200.57159 | -1.09920 | 2.257 | 4010 | 160 | 43 | - |
| 4006 | 154 | 55328 | 200.95323 | 1.68626 | 2.875 | 4710 | 107 | 15 | 1 |
| 4050 | 238 | 55599 | 201.68462 | -0.26589 | 2.372 | 3610 | 111 | 13 | K1 |
| 4839 | 78 | 55703 | 202.41447 | 5.93843 | 2.613 | 4980 | 110 | 13 | a |
| 4837 | 638 | 55707 | 203.17920 | 7.01826 | 3.179 | 4410 | 111 | 85 | - |
| 4046 | 360 | 55605 | 203.42526 | -0.26357 | 2.214 | 4030 | 112 | 26 | Z |
| 3986 | 416 | 55329 | 203.81834 | 34.80543 | 1.750 | 4070 | 105 | 15 | 1 |
| 3986 | 712 | 55329 | 204.47633 | 36.64378 | 3.272 | 2340 | 121 | 25 | - |
| 4709 | 452 | 55720 | 205.75497 | 39.56483 | 2.146 | 3050 | 155 | 11 | P |
| 3852 | 394 | 55243 | 206.93414 | 37.21049 | 2.128 | 2830 | 110 | 39 | - |
| 4864 | 532 | 55680 | 207.07887 | 6.39298 | 2.404 | 4730 | 108 | 21 | - |
| 4036 | 360 | 55330 | 208.67125 | 2.08115 | 2.576 | 4740 | 108 | 24 | K |
| 4864 | 958 | 55680 | 209.03471 | 7.50479 | 2.272 | 2090 | 140 | 46 | NaL |
| 4863 | 692 | 55688 | 210.20709 | 6.88555 | 2.296 | 4610 | 207 | 18 | S |
| 3855 | 546 | 55268 | 211.36745 | 37.03210 | 2.343 | 3970 | 116 | 12 | P1 |
| 3858 | 132 | 55273 | 212.81551 | 33.07554 | 2.561 | 3900 | 114 | 28 | K |
| 4030 | 794 | 55634 | 214.14851 | 3.13215 | 2.217 | 4410 | 106 | 14 | - |
| 4861 | 882 | 55710 | 215.83592 | 7.22793 | 2.515 | 2340 | 128 | 18 | F1 |
| 4781 | 72 | 55653 | 217.52168 | 4.30654 | 2.420 | 3420 | 150 | 16 | 1V |
| 4860 | 844 | 55691 | 217.69319 | 6.84796 | 2.221 | 2880 | 117 | 23 | 1 |
| 4860 | 872 | 55691 | 217.86386 | 7.49870 | 2.400 | 4580 | 131 | 19 | S |
| 4780 | 960 | 55682 | 219.49362 | 4.46428 | 2.119 | 3500 | 101 | 10 | P1 |
| 3868 | 978 | 55360 | 220.87230 | 32.58603 | 2.635 | 2440 | 116 | 13 | 1K |
| 3878 | 532 | 55361 | 221.68694 | 29.28241 | 2.377 | 4040 | 103 | 58 | |
| 3877 | 446 | 55365 | 224.86037 | 27.50614 | 2.878 | 4420 | 102 | 35 | Na |
| 4015 | 122 | 55624 | 225.19507 | 0.91910 | 2.295 | 3990 | 160 | 42 | S |
| 3875 | 960 | 55364 | 225.45438 | 31.12804 | 2.398 | 4920 | 750 | 13 | 1P |
| 4717 | 546 | 55742 | 225.80814 | 36.06848 | 3.333 | 2820 | 121 | 11 | - |
| 3877 | 810 | 55365 | 226.02339 | 28.88535 | 2.733 | 2150 | 118 | 127 | aN |
| 4014 | 526 | 55630 | 227.51440 | 0.07243 | 2.251 | 4780 | 104 | 13 | - |
| 4776 | 970 | 55652 | 228.44547 | 4.78620 | 3.158 | 4440 | 138 | 11 | 1 |
| 3964 | 340 | 55648 | 228.75029 | 25.17396 | 2.208 | 4530 | 108 | 19 | - |
| 3851 | 654 | 55302 | 229.28658 | 27.97025 | 2.813 | 3760 | 132 | 31 | - |

Table 4:: Table of 220 fat quasars, selected and confirmed to have broad emission lines and faint continua. All line values are for CIV. S/N represents line flux divided by error.

| Plate | Fiber | MJD | RA ° | Dec ° | z | FWHM km s$^{-1}$ | REW Å | S/N | Flag |
|---|---|---|---|---|---|---|---|---|---|
| 3964 | 56 | 55648 | 229.85526 | 25.21152 | 2.280 | 4890 | 102 | 18 | - |
| 3950 | 200 | 55680 | 230.53825 | 20.19364 | 2.715 | 4210 | 101 | 37 | NaL |
| 3954 | 270 | 55680 | 231.67892 | 23.16829 | 1.676 | 4910 | 113 | 25 | Z |
| 3944 | 789 | 55660 | 232.78375 | 21.62366 | 2.559 | 3530 | 170 | 21 | F1 |
| 3953 | 334 | 55322 | 233.37009 | 24.64289 | 2.716 | 3400 | 113 | 22 | - |
| 3947 | 516 | 55332 | 234.27441 | 25.38034 | 2.302 | 4980 | 107 | 17 | P |
| 4881 | 455 | 55733 | 234.89574 | 5.89138 | 3.185 | 4600 | 101 | 18 | F |
| 3947 | 350 | 55332 | 235.21089 | 24.97491 | 1.912 | 3430 | 104 | 33 | Z |
| 5011 | 412 | 55739 | 235.74986 | 30.44749 | 1.852 | 4950 | 124 | 22 | Z |
| 4971 | 960 | 55747 | 236.83755 | 34.39024 | 2.283 | 3070 | 113 | 21 | 1 |
| 5011 | 200 | 55739 | 237.13303 | 31.33097 | 2.731 | 3210 | 134 | 31 | NL |
| 3927 | 910 | 55333 | 237.67825 | 16.31886 | 2.360 | 4690 | 103 | 18 | - |
| 3941 | 328 | 55321 | 237.86864 | 23.06630 | 2.240 | 4780 | 100 | 16 | F |
| 5010 | 515 | 55748 | 237.90009 | 31.00244 | 2.192 | 4220 | 100 | 15 | P |
| 4726 | 912 | 55712 | 237.95831 | 30.40234 | 2.782 | 3930 | 158 | 27 | S |
| 4877 | 768 | 55707 | 238.07269 | 6.27258 | 1.783 | 4790 | 103 | 38 | Z |
| 4961 | 632 | 55719 | 240.53888 | 32.98407 | 2.228 | 3840 | 105 | 32 | - |
| 3930 | 70 | 55332 | 240.79385 | 19.88244 | 3.613 | 4750 | 120 | 34 | aNL |
| 4724 | 370 | 55742 | 241.00821 | 26.03141 | 2.204 | 4220 | 123 | 20 | - |
| 4961 | 82 | 55719 | 242.26128 | 31.20383 | 3.072 | 2820 | 115 | 27 | 1 |
| 4807 | 92 | 55687 | 243.47005 | 3.39103 | 1.560 | 4230 | 141 | 17 | Z |
| 4057 | 474 | 55357 | 243.51746 | 20.40692 | 2.615 | 3400 | 110 | 42 | SKE |
| 5007 | 890 | 55710 | 245.96747 | 29.11548 | 2.500 | 4890 | 104 | 65 | - |
| 4061 | 545 | 55362 | 247.18037 | 20.65864 | 2.937 | 3260 | 123 | 109 | aF |
| 4953 | 114 | 55749 | 247.70589 | 30.22554 | 2.357 | 4610 | 100 | 11 | PL |
| 4059 | 389 | 55360 | 251.32671 | 16.70250 | 1.617 | 3700 | 102 | 12 | Z |
| 4176 | 370 | 55682 | 253.01103 | 17.48122 | 2.935 | 2820 | 100 | 102 | ANV |
| 4996 | 496 | 55720 | 253.06999 | 29.71210 | 2.658 | 4510 | 120 | 78 | SF |
| 4987 | 680 | 55746 | 253.73090 | 35.16373 | 2.442 | 3630 | 132 | 34 | 1 |
| 4177 | 42 | 55688 | 256.97186 | 22.94650 | 2.276 | 3830 | 126 | 62 | 1 |
| 5000 | 116 | 55715 | 257.89771 | 28.45763 | 2.279 | 4250 | 103 | 108 | BH |
| 4989 | 388 | 55743 | 257.97568 | 36.56138 | 2.424 | 4870 | 122 | 11 | P |
| 5001 | 184 | 55719 | 260.15424 | 29.38494 | 2.352 | 4830 | 133 | 24 | |
| 4998 | 70 | 55722 | 260.78305 | 31.78522 | 2.826 | 2630 | 105 | 11 | 1F |

Table 4:: Table of 220 fat quasars, selected and confirmed to have broad emission lines and faint continua. All line values are for CIV. S/N represents line flux divided by error.

| Plate | Fiber | MJD | RA ° | Dec ° | z | FWHM km s$^{-1}$ | REW Å | S/N | Flag |
|---|---|---|---|---|---|---|---|---|---|
| 5004 | 530 | 55711 | 261.25562 | 27.10382 | 2.580 | 4570 | 142 | 32 | K |
| 4080 | 544 | 55471 | 320.99350 | 4.26131 | 2.238 | 4790 | 114 | 43 | aN |
| 4084 | 286 | 55447 | 322.60052 | 4.43307 | 2.613 | 3530 | 139 | 43 | 1KF |
| 4196 | 262 | 55478 | 326.34143 | -0.64358 | 2.026 | 4810 | 102 | 27 | 1 |
| 4090 | 456 | 55500 | 327.79037 | 2.68166 | 2.539 | 4440 | 165 | 17 | K |
| 4198 | 632 | 55480 | 329.24921 | 1.00068 | 2.702 | 4410 | 108 | 12 | 1K |
| 5065 | 178 | 55739 | 331.51306 | 9.10601 | 2.155 | 4460 | 124 | 18 | - |
| 4316 | 850 | 55505 | 332.01895 | 2.59414 | 3.192 | 2330 | 173 | 68 | F |
| 4201 | 450 | 55443 | 333.85004 | -0.94550 | 2.491 | 4220 | 136 | 35 | N |
| 4202 | 82 | 55445 | 337.49619 | -0.52422 | 2.754 | 3810 | 100 | 22 | S |
| 4291 | 480 | 55525 | 337.75461 | 4.00852 | 2.231 | 4700 | 123 | 12 | 1PS |
| 4209 | 510 | 55478 | 346.84720 | 0.00452 | 2.621 | 4510 | 111 | 27 | K |
| 4210 | 93 | 55444 | 350.85907 | -1.00920 | 2.349 | 3960 | 240 | 63 | N |
| 4279 | 544 | 55508 | 356.37802 | 4.96007 | 2.193 | 4150 | 103 | 22 | S |
| 4280 | 154 | 55503 | 356.75461 | 1.86590 | 2.496 | 2640 | 150 | 28 | 1 |
| 4279 | 818 | 55508 | 357.50342 | 3.84377 | 2.863 | 2710 | 117 | 38 | - |
| 4214 | 24 | 55451 | 357.90372 | -0.40829 | 2.331 | 4530 | 107 | 14 | 1 |
| 4215 | 957 | 55471 | 359.50098 | 0.76272 | 2.546 | 3340 | 125 | 41 | 1K |

### A.3. Spectra from Fat Quasar Sample

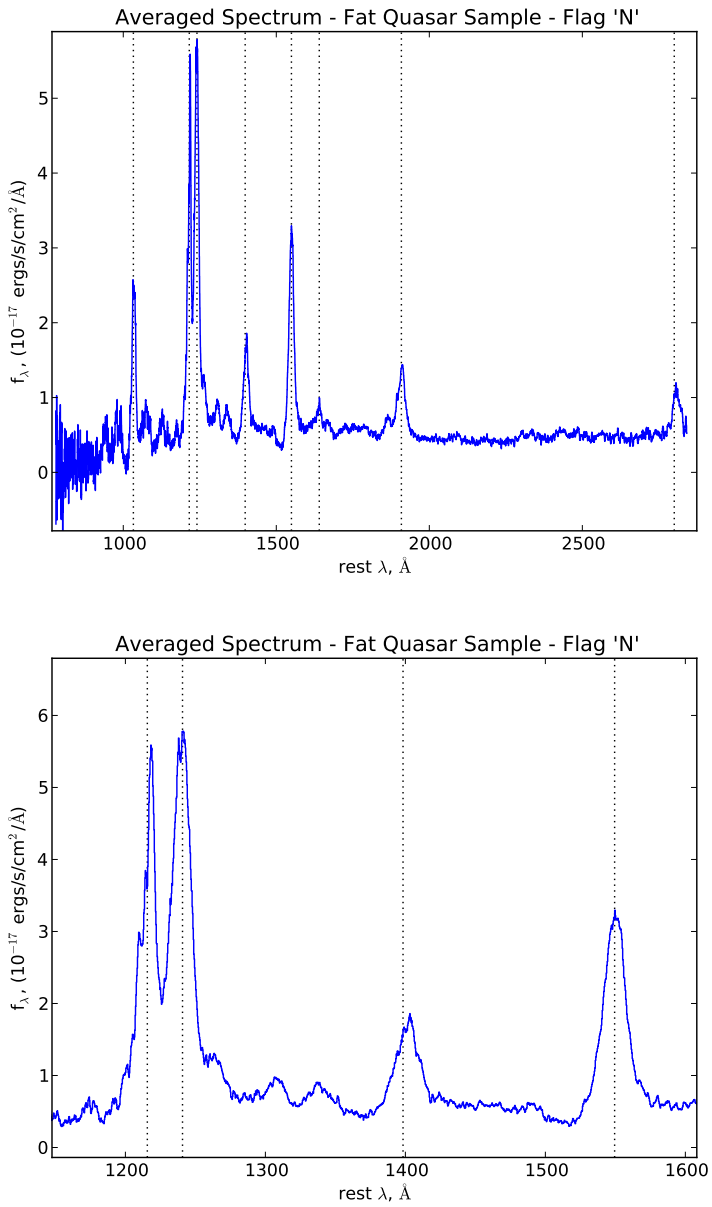


Fig. 9.— The averaged spectrum of all quasars in the fat sample which were given the flag letter "N", indicating excessively strong NV emission (an individual example is shown in Fig. 12). To see an averaged spectrum for all fat quasar candidates, see Fig. 6. *Upper*: The entire averaged spectrum, over the rest-frame wavelength range observed. Note the flat, faint continuum level throughout the spectrum. However, slight absorption blue-ward of several lines can be noticed. Identified spectral lines are, from left to right: Ly$\beta$, Ly$\alpha$, NV, SiIV + OIV] (a combined line), CIV, HeII, CIII], and MgII. *Lower*: The same averaged spectrum, focusing on the wavelength range around Ly$\alpha$ and CIV. Identified spectral lines are, from left to right: Ly$\alpha$, NV, SiIV + OIV], and CIV. Notice the incredibly large amplitude of NV relative to Ly$\alpha$. It is possible that NV possesses a similar absorption trough as the other lines seen above, resulting in significant attenuation of Ly$\alpha$.

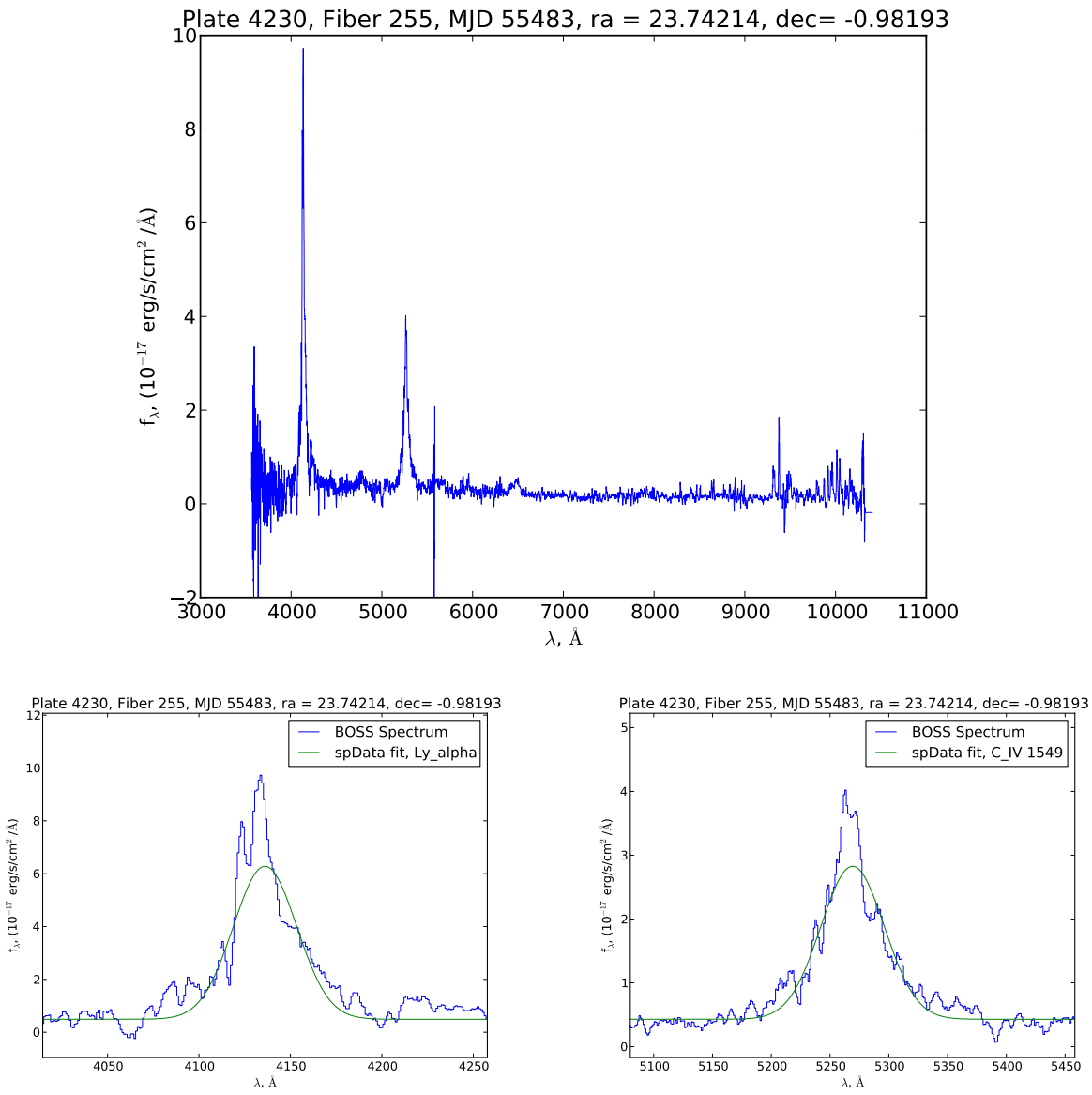


Fig. 10.— The spectrum of a fat quasar in the final sample. The redshift of the object is z = 2.401. *Upper*: The continuum of the quasar is very faint and flat, indicative of an obscured, Type II quasar. *Lower*: The Ly$\alpha$ (*left*) and CIV (*right*) lines are fairly broad, with FWHM of 2970 and 3620 $\mathrm{km\,s^{-1}}$ respectively, indicative of an unobscured, Type I quasar. This quasar was given no flag.

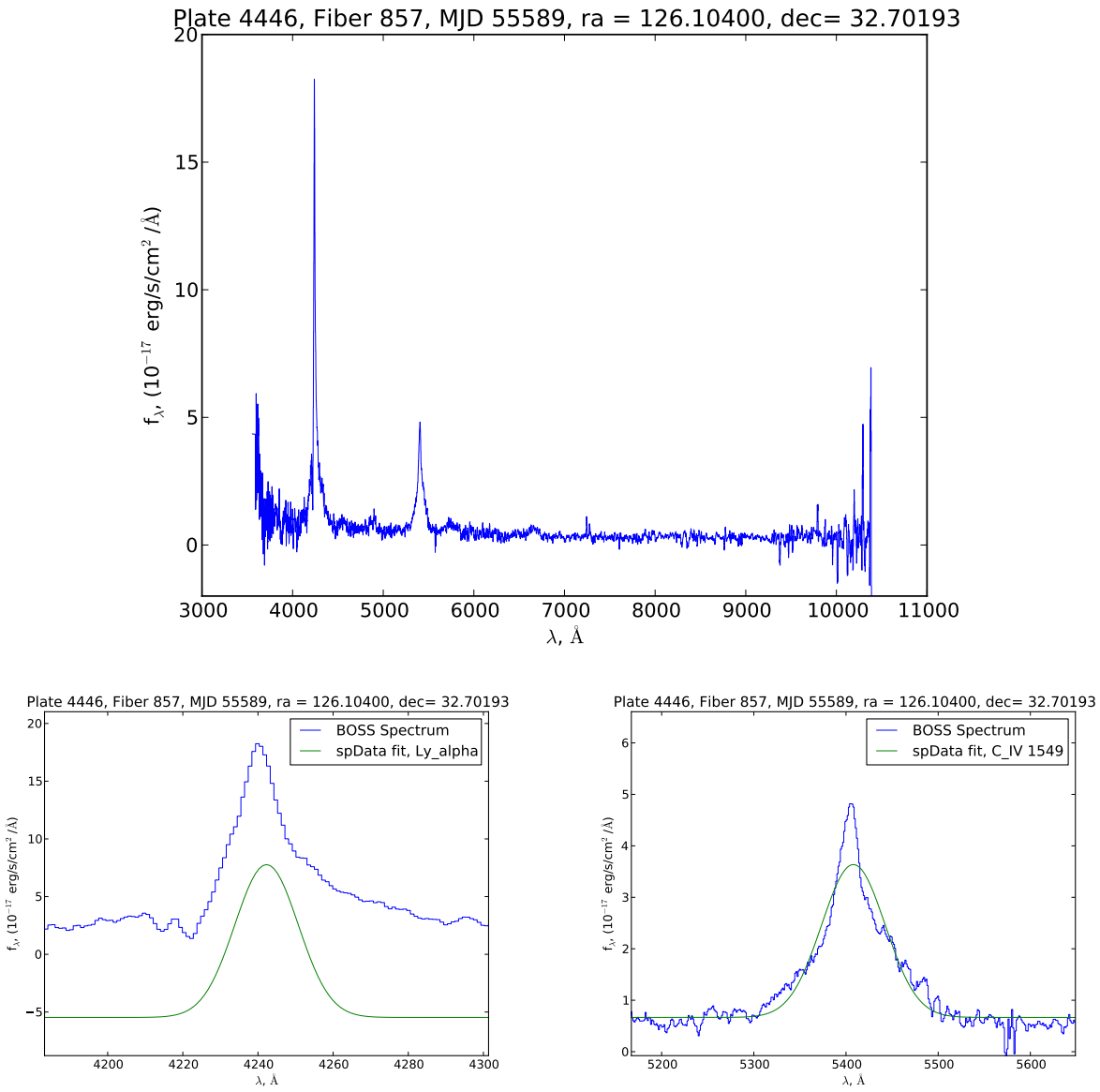


Fig. 11.— The spectrum of a fat quasar in the final sample. The redshift of the object is z = 2.490. *Upper*: The continuum of the quasar is faint and flat, indicative of an obscured, Type II quasar. *Lower*: The CIV (*right*) line is very broad, with FWHM of 4490 $\mathrm{km\,s^{-1}}$ indicative of an unobscured, Type I quasar. Note that the Ly$\alpha$ (*left*) line continuum is improperly matched by the BOSS continuum, which was a common occurrence in our sample (nearly 20% of objects). This quasar was given flag "1".

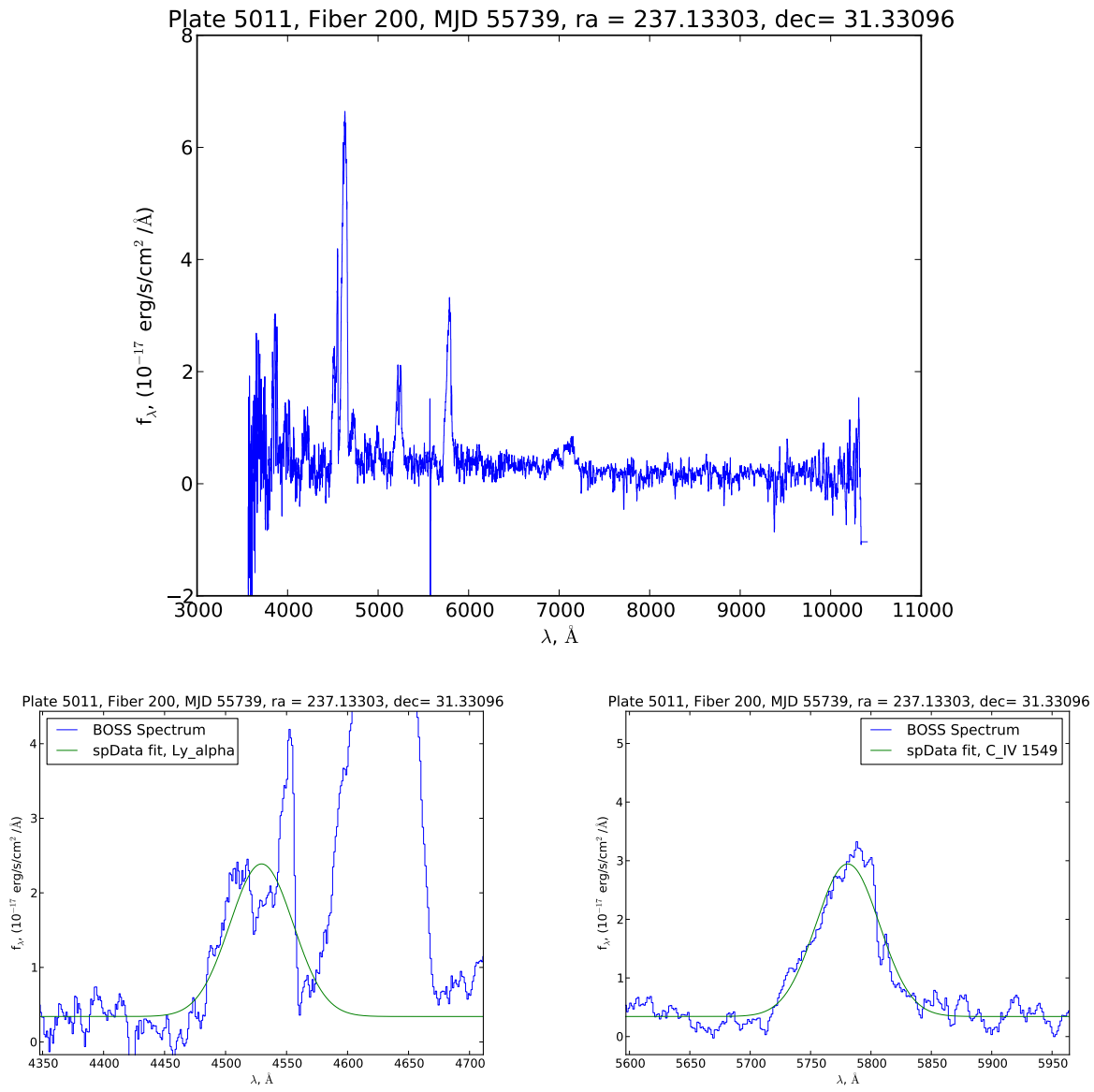


Fig. 12.— The continuum of a fat quasar in the final sample. The redshift of the object is z = 2.731. *Upper*: The spectrum of the quasar is faint and flat, indicative of an obscured, Type II quasar. *Lower*: The CIV (*right*) line is broad, with FWHM of 3210 $\mathrm{km\,s^{-1}}$ indicative of an unobscured, Type I quasar. Note that the Ly$\alpha$ (*left*) line has been partly absorbed away by an extremely strong NV line. This quasar was given flag "bLN".

### A.4. Objects Removed from the Sample

Table 5:: 15 Quasars removed from initial sample of 235 fat quasar candidates.

| Plate | Fiber | MJD | Flag |
|---|---|---|---|
| 4389 | 690 | 55539 | XBHaNL |
| 4504 | 378 | 55571 | XLaH |
| 4801 | 296 | 55653 | XHaL |
| 3772 | 306 | 55277 | XBaHZ |
| 4623 | 488 | 55621 | XP |
| 3849 | 758 | 55274 | XBHaL |
| 3850 | 710 | 55575 | XZP |
| 3979 | 982 | 55597 | XPZ |
| 4785 | 6 | 55659 | XaKLP |
| 3953 | 970 | 55322 | XNaLK |
| 4056 | 380 | 55357 | XaLN |
| 4181 | 692 | 55685 | XaLN |
| 4997 | 512 | 55738 | XaL |
| 4319 | 132 | 55507 | XBaL |
| 4206 | 747 | 55471 | XHB |

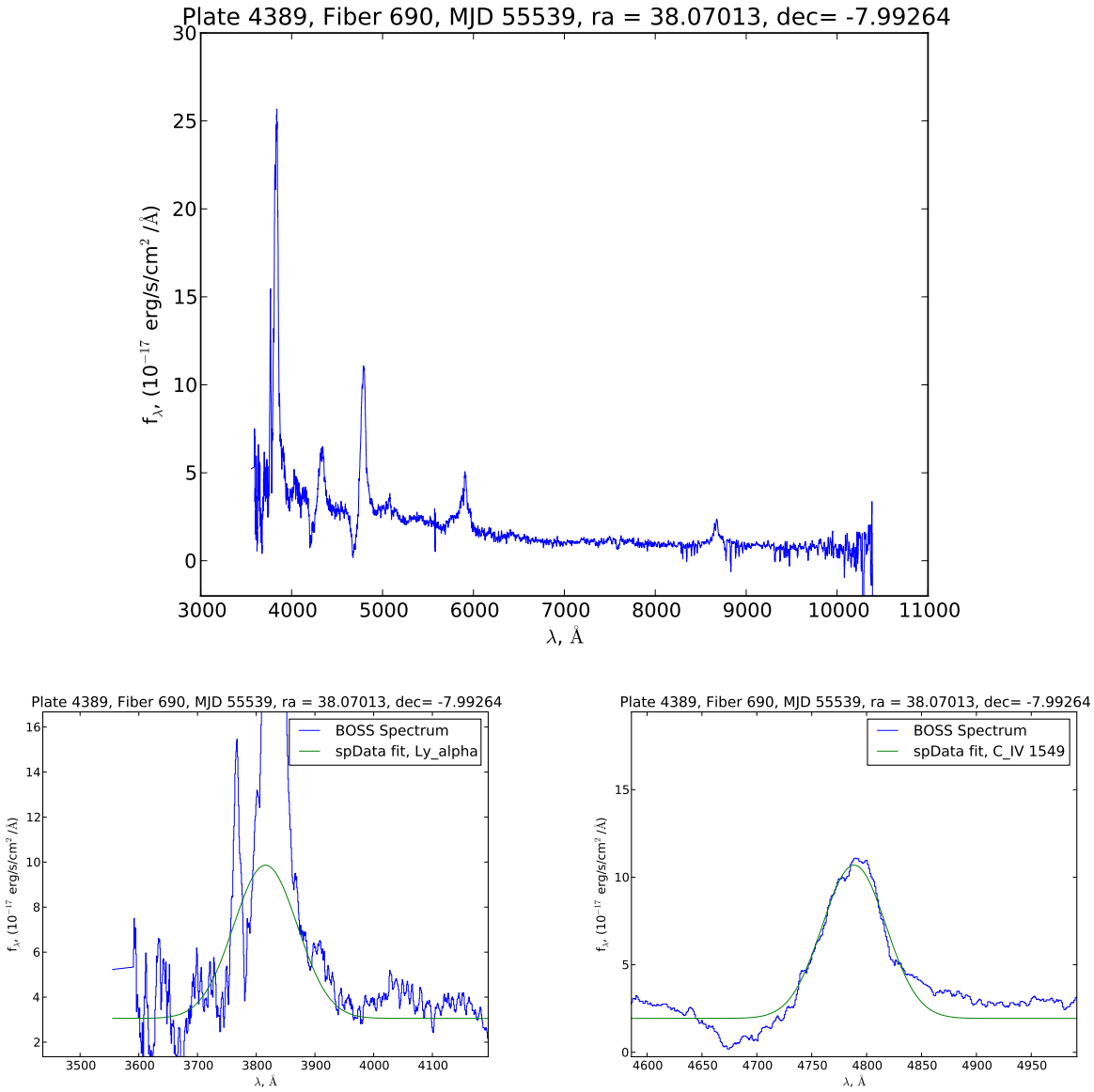


Fig. 13.— The spectrum of a quasar which was removed from the original sample, for possessing a bright, blue continuum and evidence of BAL-type absorption. The redshift of the object is z = 2.097. *Upper*: The continuum of the quasar is high and very clearly sloping blue-ward. Notice the deep absorption features blue-ward of SiIV ( 4300Å) and CIV ( 4800Å), indicative of a Broad-Absorption Line quasar. *Lower*: The Ly$\alpha$ (*left*) and CIV (*right*) lines. This quasar was given a flag of "XBHaNL".

## B. SDSS-III File Types Used

As described in §2.2, each of the following file types are organized by spectroscopic plate (4 digit integer) and Modified Julian Date (5 digit integer). Within a given file, objects are labeled by fiber number 1-1000.

### B.1. spPlate

spPlate files hold the reduced spectra for all 1000 fibers of each plate. The primary HDU holds the spectral flux, in units of $10^{-17}$ erg $s^{-1}$ $cm^{-2}$ $Å^{-1}$. The extension HDUs hold, among other data, the inverse variance in the flux and the average sky background flux which was subtracted.

### B.2. spZbest

spZbest files contain the general spectroscopic classifications for each spectrum as a whole, derived by the BOSS pipeline. Important data available in this file include the pipeline redshift of the quasar, its RA/Dec position, and object class.

### B.3. spZline

spZline files contain detailed information measured on 33 important spectral lines for each of the 1000 objects on the plate. Each row, thus, corresponds to a single line for a single object, and each object will have 33 rows associated with it. Important lines include Ly$\alpha$, CIV, and NV, and important data found on this file includes the Gaussian width ($km\,s^{-1}$), equivalent width (Å), and area in the Gaussian fit, derived for each emission line for all objects.

## REFERENCES

Ahn, C. P., Alexandroff, R., Allende Prieto, C., Anderson, S. F., Anderton, T., Andrews, B. H., Aubourg, É., Bailey, S., Balbinot, E., Barnes, R., & et al. 2012, ApJS, 203, 21

Alexandroff, R. 2012, Senior Thesis, Princeton University

Alexandroff, R., Strauss, M. A., Greene, J. E., Zakamska, N. L., Ross, N. P., Brandt, W. N., & Liu, G. In Preparation

Bolton, A. S., Schlegel, D. J., Aubourg, E., Bailey, S., Bhardwaj, V., Brownstein, J. R., Burles, S., Chen, Y.-M., Dawson, K., Eisenstein, D. J., Gunn, J. E., Knapp, G. R., Loomis, C. P., Lupton, R. H., Maraston, C., Muna, D., Myers, A. D., Olmstead, M. D., Padmanabhan,

N., Pâris, I., Percival, W. J., Petitjean, P., Rockosi, C. M., Ross, N. P., Schneider, D. P., Shu, Y., Strauss, M. A., Thomas, D., Tremonti, C. A., Wake, D. A., Weaver, B. A., & Wood-Vasey, W. M. 2012, The Astronomical Journal, 144, 144

Eisenstein, D. J., Weinberg, D. H., Agol, E., Aihara, H., Allende Prieto, C., Anderson, S. F., Arns, J. A., Aubourg, É., Bailey, S., Balbinot, E., & et al. 2011, AJ, 142, 72

Gunn, J. E., Carr, M., Rockosi, C., Sekiguchi, M., Berry, K., Elms, B., de Haas, E., Ivezić, Ž., Knapp, G., Lupton, R., Pauls, G., Simcoe, R., Hirsch, R., Sanford, D., Wang, S., York, D., Harris, F., Annis, J., Bartozek, L., Boroski, W., Bakken, J., Haldeman, M., Kent, S., Holm, S., Holmgren, D., Petravick, D., Prosapio, A., Rechenmacher, R., Doi, M., Fukugita, M., Shimasaku, K., Okada, N., Hull, C., Siegmund, W., Mannery, E., Blouke, M., Heidtman, D., Schneider, D., Lucinio, R., & Brinkman, J. 1998, AJ, 116, 3040

Gunn, J. E., Siegmund, W. A., Mannery, E. J., Owen, R. E., Hull, C. L., Leger, R. F., Carey, L. N., Knapp, G. R., York, D. G., Boroski, W. N., Kent, S. M., Lupton, R. H., Rockosi, C. M., Evans, M. L., Waddell, P., Anderson, J. E., Annis, J., Barentine, J. C., Bartoszek, L. M., Bastian, S., Bracker, S. B., Brewington, H. J., Briegel, C. I., Brinkmann, J., Brown, Y. J., Carr, M. A., Czarapata, P. C., Drennan, C. C., Dombeck, T., Federwitz, G. R., Gillespie, B. A., Gonzales, C., Hansen, S. U., Harvanek, M., Hayes, J., Jordan, W., Kinney, E., Klaene, M., Kleinman, S. J., Kron, R. G., Kresinski, J., Lee, G., Limmongkol, S., Lindenmeyer, C. W., Long, D. C., Loomis, C. L., McGehee, P. M., Mantsch, P. M., Neilsen, Jr., E. H., Neswold, R. M., Newman, P. R., Nitta, A., Peoples, Jr., J., Pier, J. R., Prieto, P. S., Prosapio, A., Rivetta, C., Schneider, D. P., Snedden, S., & Wang, S.-i. 2006, AJ, 131, 2332

Hopkins, P. F., Hernquist, L., Cox, T. J., Di Matteo, T., Robertson, B., & Springel, V. 2006, ApJS, 163, 1

Hunter, J. D. 2007, Computing In Science & Engineering, 9, 90

Pâris, I., Petitjean, P., Aubourg, E., Bailey, S., Ross, N. P., Myers, A. D., Strauss, M. A., Anderson, S. F., Arnau, E., Bautista, J., Bizyaev, D., Bolton, A. S., Bovy, J., Brandt, W. N., Brewington, H., Browstein, J. R., Busca, N., Capellupo, D., Carithers, W., Croft, R. A. C., Dawson, K., Delubac, T., Ebelke, G., Eisenstein, D. J., Engelke, P., Fan, X., Filiz Ak, N., Finley, H., Font-Ribera, A., Ge, J., Gibson, R. R., Hall, P. B., Hamann, F., Hennawi, J. F., Ho, S., Hogg, D. W., Ivezić, v., Jiang, L., Kimball, A. E., Kirkby, D., Kirkpatrick, J. A., Lee, K.-G., Le Goff, J.-M., Lundgren, B., MacLeod, C. L., Malanushenko, E., Malanushenko, V., Maraston, C., McGreer, I. D., McMahon, R. G., Miralda-Escudé, J., Muna, D., Noterdaeme, P., Oravetz, D., Palanque-Delabrouille, N., Pan, K., Perez-Fournon, I., Pieri, M. M., Richards, G. T., Rollinde, E., Sheldon, E. S., Schlegel, D. J., Schneider, D. P., Slosar, A., Shelden, A., Shen, Y., Simmons, A., Snedden, S., Suzuki, N., Tinker, J., Viel, M., Weaver, B. A., Weinberg, D. H., White, M., Wood-Vasey, W. M., & Yèche, C. 2012, Astronomy & Astrophysics, 548, A66

Ross, N. P., Myers, A. D., Sheldon, E. S., Yèche, C., Strauss, M. A., Bovy, J., Kirkpatrick, J. A., Richards, G. T., Aubourg, É., Blanton, M. R., Brandt, W. N., Carithers, W. C., Croft, R. A. C., da Silva, R., Dawson, K., Eisenstein, D. J., Hennawi, J. F., Ho, S., Hogg, D. W., Lee, K.-G., Lundgren, B., McMahon, R. G., Miralda-Escudé, J., Palanque-Delabrouille, N., Pâris, I., Petitjean, P., Pieri, M. M., Rich, J., Roe, N. A., Schiminovich, D., Schlegel, D. J., Schneider, D. P., Slosar, A., Suzuki, N., Tinker, J. L., Weinberg, D. H., Weyant, A., White, M., & Wood-Vasey, W. M. 2012, ApJS, 199, 3

Schmidt, M. 1963, Nature, 197, 1040

Vanden Berk, D. E., Richards, G. T., Bauer, A., Strauss, M. A., Schneider, D. P., Heckman, T. M., York, D. G., Hall, P. B., Fan, X., Knapp, G. R., Anderson, S. F., Annis, J., Bahcall, N. A., Bernardi, M., Briggs, J. W., Brinkmann, J., Brunner, R., Burles, S., Carey, L., Castander, F. J., Connolly, A. J., Crocker, J. H., Csabai, I., Doi, M., Finkbeiner, D., Friedman, S., Frieman, J. A., Fukugita, M., Gunn, J. E., Hennessy, G. S., Ivezić, Ž., Kent, S., Kunszt, P. Z., Lamb, D. Q., Leger, R. F., Long, D. C., Loveday, J., Lupton, R. H., Meiksin, A., Merelli, A., Munn, J. A., Newberg, H. J., Newcomb, M., Nichol, R. C., Owen, R., Pier, J. R., Pope, A., Rockosi, C. M., Schlegel, D. J., Siegmund, W. A., Smee, S., Snir, Y., Stoughton, C., Stubbs, C., SubbaRao, M., Szalay, A. S., Szokoly, G. P., Tremonti, C., Uomoto, A., Waddell, P., Yanny, B., & Zheng, W. 2001, AJ, 122, 549

Wright, E. L., Eisenhardt, P. R. M., Mainzer, A. K., Ressler, M. E., Cutri, R. M., Jarrett, T., Kirkpatrick, J. D., Padgett, D., McMillan, R. S., Skrutskie, M., Stanford, S. A., Cohen, M., Walker, R. G., Mather, J. C., Leisawitz, D., Gautier, III, T. N., McLean, I., Benford, D., Lonsdale, C. J., Blain, A., Mendez, B., Irace, W. R., Duval, V., Liu, F., Royer, D., Heinrichsen, I., Howard, J., Shannon, M., Kendall, M., Walsh, A. L., Larsen, M., Cardon, J. G., Schick, S., Schwalm, M., Abid, M., Fabinsky, B., Naes, L., & Tsai, C.-W. 2010, AJ, 140, 1868

York, D. G., Adelman, J., Anderson, Jr., J. E., Anderson, S. F., Annis, J., Bahcall, N. A., Bakken, J. A., Barkhouser, R., Bastian, S., Berman, E., Boroski, W. N., Bracker, S., Briegel, C., Briggs, J. W., Brinkmann, J., Brunner, R., Burles, S., Carey, L., Carr, M. A., Castander, F. J., Chen, B., Colestock, P. L., Connolly, A. J., Crocker, J. H., Csabai, I., Czarapata, P. C., Davis, J. E., Doi, M., Dombeck, T., Eisenstein, D., Ellman, N., Elms, B. R., Evans, M. L., Fan, X., Federwitz, G. R., Fiscelli, L., Friedman, S., Frieman, J. A., Fukugita, M., Gillespie, B., Gunn, J. E., Gurbani, V. K., de Haas, E., Haldeman, M., Harris, F. H., Hayes, J., Heckman, T. M., Hennessy, G. S., Hindsley, R. B., Holm, S., Holmgren, D. J., Huang, C.-h., Hull, C., Husby, D., Ichikawa, S.-I., Ichikawa, T., Ivezić, Ž., Kent, S., Kim, R. S. J., Kinney, E., Klaene, M., Kleinman, A. N., Kleinman, S., Knapp, G. R., Korienek, J., Kron, R. G., Kunszt, P. Z., Lamb, D. Q., Lee, B., Leger, R. F., Limmongkol, S., Lindenmeyer, C., Long, D. C., Loomis, C., Loveday, J., Lucinio, R., Lupton, R. H., MacKinnon, B., Mannery, E. J., Mantsch, P. M., Margon, B., McGehee, P., McKay, T. A., Meiksin, A., Merelli, A.,

Monet, D. G., Munn, J. A., Narayanan, V. K., Nash, T., Neilsen, E., Neswold, R., Newberg, H. J., Nichol, R. C., Nicinski, T., Nonino, M., Okada, N., Okamura, S., Ostriker, J. P., Owen, R., Pauls, A. G., Peoples, J., Peterson, R. L., Petravick, D., Pier, J. R., Pope, A., Pordes, R., Prosapio, A., Rechenmacher, R., Quinn, T. R., Richards, G. T., Richmond, M. W., Rivetta, C. H., Rockosi, C. M., Ruthmansdorfer, K., Sandford, D., Schlegel, D. J., Schneider, D. P., Sekiguchi, M., Sergey, G., Shimasaku, K., Siegmund, W. A., Smee, S., Smith, J. A., Snedden, S., Stone, R., Stoughton, C., Strauss, M. A., Stubbs, C., SubbaRao, M., Szalay, A. S., Szapudi, I., Szokoly, G. P., Thakar, A. R., Tremonti, C., Tucker, D. L., Uomoto, A., Vanden Berk, D., Vogeley, M. S., Waddell, P., Wang, S.-i., Watanabe, M., Weinberg, D. H., Yanny, B., Yasuda, N., & SDSS Collaboration. 2000, AJ, 120, 1579

Zakamska, N. L., Strauss, M. A., Krolik, J. H., Collinge, M. J., Hall, P. B., Hao, L., Heckman, T. M., eljko Ivezi, Richards, G. T., Schlegel, D. J., Schneider, D. P., Strateva, I., Vanden Berk, D. E., Anderson, S. F., & Brinkmann, J. 2003, The Astronomical Journal, 126, 2125